International Journal of Hydrogen Energy 191 (2025) 152228

Contents lists available at ScienceDirect

International Journal of Hydrogen Energy

journal homepage: www.elsevier.com/locate/he

Hydrogen utilization for decarbonizing the dairy industry: A techno-economic scenario analysis

Marco Puglia [a,*], Simone Boccaletti [b], Ahmet Fatih Kaya [a], Nicolò Morselli [a], Giulio Allesina [a], Simone Pedrazzi [a]

[a] Department of Engineering "Enzo Ferrari", Università degli Studi di Modena e Reggio Emilia, Modena, Italy
[b] Department of Economics and Social Sciences (DISES), Università Cattolica del Sacro Cuore, Piacenza, Italy

ARTICLE INFO

Handling editor: Suleyman I. Allakhverdiev

Keywords:
Green hydrogen
Steam generation
Dairy industry
Agro-industrial decarbonization
Techno-economic analysis
Sustainable food production

ABSTRACT

This study investigates the integration of on-site green hydrogen as a substitute for methane in steam generation in the dairy industry, specifically in the production of Parmigiano Reggiano cheese. This represents a novel application of green hydrogen in industrial dairy processing, with the potential to reduce greenhouse gas emissions. Hydrogen is assumed to be generated via electrolysis powered by photovoltaic energy. A comprehensive techno-economic assessment was conducted, with simulations covering key design variables such as hydrogen fraction in steam production, photovoltaic panel orientation, and storage pressure. A wide range of scenarios was defined in order to account for variability in system structures and performance, and a comprehensive economic assessment was then carried out using a Monte Carlo simulation approach and a sensitivity analysis. Results indicate that, in all scenarios, the net present value over a 15-year period remains negative when benefits are limited to methane savings. Indeed, the high capital expenditure associated with hydrogen systems presents a major barrier. The most favorable cases occur at low hydrogen shares with seasonal storage, while full conversion to hydrogen maximizes CO_2 abatement but is least economical. With public funding, the emissions saved per euro of public support range from 1.58 to 2.14 kg CO_{2eq}/€.

Nomenclature

Abbreviations	
CAPEX	Capital Expenditure
CFD	Computational Fluid Dynamics
CH_4	Methane
CO_2eq	Carbon dioxide equivalent
comp	Compressor
conv	Converter
CSP	Concentrated Solar Power
DC	Direct Current
DHI	Diffuse Horizontal Irradiance (W/m^2)
DNI	Direct Normal Irradiance (W/m^2)
el	Electrolyser
ESPS	Emissions Saved per Euro of Public Support (kgCO_2eq/€)
FAO	Food and Agriculture Organization of the United Nations
GHG	Greenhouse Gas
GHI	Global Horizontal Irradiance (W/m^2)
GWP	Global Warming Potential
H_2	Hydrogen
HENG	Hydrogen-Enriched Natural Gas
HHV	Higher Heating Value (kWh/kg or MJ/m^3)
IPCC	Intergovernmental Panel on Climate Change
LCOE	Levelized Cost of Energy
max	Maximum value
min	Minimum value
NPB	Net Present Benefit (€)
NPTC	Net Present Total Cost (€)
NPV	Net Present Value (€)
O&M	Operation and Maintenance
PEMFC	Proton Exchange Membrane Fuel Cell
PFR	Minimum Public Funding Rate (%)
PV	Photovoltaic
PVGIS	Photovoltaic Geographical Information System
R_{Lc}	Residual life of component c (years)
R_{vc}	Residual value of component c (€)
SAM	System Advisor Model
T_{LC}	Total life of component c (years)

(continued on next column)

(continued on next page)

* Corresponding author. Department of Engineering "Enzo Ferrari", Università degli Studi di Modena e Reggio Emilia, Modena, Italy
E-mail address: marco.puglia@unimore.it (M. Puglia).

https://doi.org/10.1016/j.ijhydene.2025.152228
Received 14 July 2025; Received in revised form 15 October 2025; Accepted 24 October 2025
Available online 1 November 2025
0360-3199/© 2025 The Authors. Published by Elsevier Ltd on behalf of Hydrogen Energy Publications LLC. This is an open access article under the CC BY license (http://creativecommons.org/licenses/by/4.0/).

(*continued*)

Abbreviations	
TMY	Typical Meteorological Year
Greek Letters	
δ	Discount rate
η	Efficiency
ν	Inflation rate
ρ	Density (kg/m^3)
ω	Mass fraction
Lower-case Roman	
b	Boiler
c	component
c_p	Specific heat at constant pressure
d	Daily storage scenario
f	Volumetric fraction of hydrogen in the fuel mixture (%)
k	Ratio of specific heats
$\dot{n}$	Molar flow rate
m	Mass
$\dot{m}$	Mass flow rate (kg/s)
p	Pressure
s	Seasonal storage scenario
v	Volume (m^3)
Upper-case Roman	
F	Faraday constant
I	Current (A)
N	Number
P	Power (kW)
Q	Thermal energy demand (kWh or GWh/year)
S	Storage size (kg or m^3)
T	Temperature (°C or K)
V	Voltage (V)

1. Introduction

The dairy sector accounts for approximately 4 % of global anthropogenic greenhouse gas emissions [1,2]. According to the Food and Agriculture Organization of the United Nations (FAO), cheese consumption has been steadily increasing in recent years, a trend that is expected to continue. In Italy alone, approximately 13 million tonnes of milk are processed annually to produce more than one million tonnes of cheese [3]. The cheese-making industry requires substantial amounts of raw materials, water, and energy, leading to significant environmental impacts [4]. Among these processes, milk pasteurization and heating are particularly energy-intensive, with thermal energy requirements ranging from 0.1 MJ/kg for soft cheeses with short ripening times and high water content to as much as 8 MJ/kg for other varieties [3]. Given this high energy demand, increasing the integration of renewable energy sources into milk processing is essential [3].

In this context, hydrogen presents a promising solution for decarbonizing thermal processes in the dairy industry. Hydrogen combustion generates zero direct carbon emissions, and depending on its production method, it can significantly reduce CO_2 emissions [5]. Green hydrogen, produced through water electrolysis powered by renewable energy sources, has been recognized as a viable option as a sustainable energy carrier for decarbonizing hard-to-abate sectors such as steel, cement, and chemicals [5,6].

Several studies have explored the techno-economic feasibility of green hydrogen production from renewable energy sources. Mostafaeipou et al. [7] conducted an evaluation of the economic viability of utilizing wind energy for the generation of electricity and hydrogen in four cities in Iran. Their research examined the potential for wind power by employing the energy pattern factor and Weibull distribution, in addition to performing an economic analysis of both 3.5 kW and 100 kW wind turbines. Focusing on a specific high-potential region, Rehman et al. [8] performed a techno-economic evaluation for an onshore wind farm in the Aqaba Gulf, determining the optimal sizing of the electrolyser and storage systems to produce green hydrogen at a levelized cost of 5.26 $/kg. In a similar techno-economic study focused on a renewable energy hub in Vietnam, Minh et al. [9] utilized the HOMER optimization model to determine the optimal configuration of a hybrid solar and wind system, achieving a Levelized Cost of Hydrogen of $5.37/kg while producing 300 kg of hydrogen per day. Similarly, Shboul et al. [10] conducted a comprehensive techno-enviro-economic analysis of a hybrid PV-Fuel Cell system for green hydrogen and power production, utilizing detailed numerical modeling in MATLAB/Simulink and machine learning methods for performance optimization. In related optimization-oriented research, Abd Elaziz et al. [11] employed a hybrid approach combining machine learning with metaheuristic optimization techniques, notably utilizing the mayfly optimization algorithm, to forecast the operational performance of an integrated solar photovoltaic–thermal (PV/T) system coupled with an electrolytic hydrogen generation unit. Investigating a different economic framework to improve sustainability, Vance et al. [12] performed a techno-economic optimization utilizing curtailed renewable energy in Ireland. Their findings indicated that the levelized cost of hydrogen might vary between 1.20 and 9.39 €/kg, contingent upon prospective renewable energy capacity and grid limitations. Lastly, Okonkwo et al. [13] investigated different off-grid energy solutions to produce hydrogen for a refueling station in Oman using HOMER software. The results showed that the most cost-effective hybrid system is: photovoltaic – wind turbine – fuel cell combination.

Within the agricultural sector specifically, various applications for on-site hydrogen have been explored. Yamaguchi et al. [14] implemented a hydroponic system for growing lettuce, powered by a hybrid energy configuration combining a hydrogen fuel cell and a lead-acid battery. Nguyen and Matsuhashi [15] utilized wind turbines and photovoltaic (PV) panels to generate electricity for a shrimp farm, using excess energy to produce hydrogen for ammonia-based fertilizer production. Carroquino et al. [16] examined a renewable energy system at a vineyard in Spain, where surplus PV energy was used to produce hydrogen for refueling hybrid fuel cell electric vehicles. Farhani et al. [17] investigated the combination of photovoltaic and fuel cell technologies within a self-sufficient hybrid energy system tailored for an agricultural farm located in Kairouan, Tunisia. Temiz and Dincer [18] introduced an “agri-CSP” system that merges solar photovoltaic technology with concentrated solar power to produce electricity, process heat, fresh water, and hydrogen. Janke et al. [19] assessed the feasibility of on-site hydrogen production for farm vehicles in Sweden, while Ceylan and Devrim [20] proposed a PV-integrated hydrogen system for electricity and heat generation in greenhouses. Al-Ali et al. [21] investigated the contribution of renewable hydrogen to the energy transition within agricultural communities in Glensaugh, Scotland. Their study evaluated two configurations of renewable hydrogen, Solar-H_2 and Wind-H_2, aimed at fulfilling energy requirements for residential, commercial, and transportation sectors by utilizing excess renewable energy storage. Beyond direct electrolysis from solar and wind, other green hydrogen production methods have been investigated in the existing literature. For instance, geothermal energy has been investigated as a potential source for hydrogen production [22,23], while biological hydrogen production methods, such as photo-fermentation using bacteria has been examined by other researchers [24]. Additionally, biomass-based hydrogen production, utilizing processes like gasification has been studied as an alternative approach [25,26]. Various strategies underscore the extensive array of approaches for incorporating hydrogen into sustainable energy systems for agriculture.

Hydrogen use in industrial or domestic boilers has also been explored. Schiro et al. [27] compared CO_2 emissions from different fuels, highlighting the advantages of hydrogen-enriched natural gas (HENG). Wang et al. [28] examined the efficiency and emissions of an industrial boiler fuelled with varying hydrogen-methane ratios. Bălănescu and Homutescu [29] studied a 25 kW condensing boiler using hydrogen-methane mixtures, finding improved condensation efficiency with higher hydrogen content.

Building on the advantages in natural gas condensing boilers, Yang et al. [30] evaluated a 2.8 MW unit and found that H_2 enrichment significantly boosts thermal efficiency, increasing it from 101.83 % to

110.60 % (based on Lower Heating Value) as the hydrogen share rises from 0 to 100 %, and confirmed that the existing condenser could manage the increased latent heat recovery without modification. Cellek and Pınarbaşı [31] conducted CFD simulations to evaluate the impact of hydrogen content on emissions and performance in a 1085 kW low-swirl boiler, reporting a reduction in fuel consumption when switching to 100 % hydrogen. Xin et al. [32] further analysed combustion characteristics in a swirl burner, demonstrating increased combustion temperature and reduced CO_2 emissions with higher hydrogen ratios. Boulahlib et al. [33] utilized a 15 kW domestic boiler with varying methane-hydrogen blending ratios (0–45 %) to investigate the emission values of NO_x, CO_2, CO, and C_xH_y, as well as the thermal performance. Wang et al. [34] utilized a 4.2 MW gas-fired boiler powered by HENG as a case study to examine its thermodynamic properties and pollutants emission. The findings indicated that the inclusion of an external economizer enhanced the overall thermal efficiency of the system by 0.4 %–0.7 %. Cheng et al. [35] conducted an extensive CFD simulation to examine the combustion characteristics in industrial boilers. Their research confirmed that higher levels of hydrogen doping result in elevated combustion temperatures and a notable decrease in CO concentration, while also observing an increase in NOx emissions.

This research evaluates the practicality of incorporating green hydrogen as a partial replacement for methane in the steam generation process used in the production of Parmigiano Reggiano cheese. Parmigiano Reggiano is a semi-fat, extra-hard cheese made from raw cow's milk, requiring a long ripening period. Its production follows a strict process, carried out in select provinces of northern Italy [36]. Currently, methane is the main fuel utilized for steam production, which is essential for the coagulation of milk and the cooking process in bell-shaped copper vats [37]. Despite the widespread use of methane, some producers continue to operate diesel-fired burners. To evaluate the feasibility of hydrogen integration, various hydrogen-methane blending ratios were analysed for fuelling the steam boiler in a Parmigiano Reggiano cheese production facility. The energy demand and, consequently, the boiler specifications were determined through an extensive assessment of multiple cheese factories in the region, also determining the characteristics of key system components, including the required number of PV panels (N_{PV}), PV system capacity in kWp (P_{PV}), electrolyser power (P_{el}), compressor power (P_{comp}), DC-DC converter capacity (P_{conv}), as well as the necessary hydrogen storage volume in cubic meters (S_v) and storage capacity in kilograms (S_m). Additionally, electrolyser efficiency (η_{el}) was computed for different system configurations. The solar power system was simulated using the System Advisor Model (SAM) software, while the alkaline electrolyser was modelled via MATLAB/Simulink.

This study addresses a critical gap in sustainable energy integration by providing an end-to-end techno-economic assessment of green hydrogen to supply process heat in the dairy industry. The analysis explicitly models PV-powered electrolysis, compression and storage, and hydrogen–methane boiler operation, quantifying system sizing, costs, uncertainty, and emissions impacts. In contrast to prior work that focuses on hydrogen production for sale or examines agro-livestock systems at a broad sectoral level without process-specific appraisal [38,39] the present study evaluates the practical advantages and limitations of on-site hydrogen generation and utilization for a defined dairy process (steam demand in Parmigiano Reggiano production). Although the case study is sector-specific, the methodology and most findings are applicable to other industries with methane-fired thermal loads seeking decarbonization via renewable-hydrogen-based process heat.

2. Materials and methods

This study proposes a model for a hydrogen production, storage, and utilization system designed to support the thermal energy requirements of Parmigiano Reggiano cheese manufacturing, either by supplementing or replacing the use of methane. Hydrogen production is assumed to originate from solar photovoltaic energy, which powers electrolysers. The produced hydrogen can be used immediately or stored, depending on the balance between production and demand, and the specific thermal requirements at any given time. To capture the wide range of potential conditions that could significantly affect the feasibility and economic viability of hydrogen implementation, a comprehensive set of scenarios was analysed. These scenarios accounted for several key factors, including the volumetric fraction of hydrogen f used in steam generation, the tilt and azimuth angles of the photovoltaic system, and the operating pressure of the hydrogen storage system. Finally, a detailed economic analysis was conducted to assess the cost implications and overall practicality of the various scenarios.

2.1. Energy load calculation

First, it was necessary to identify a quantitative indicator to be used for the energy load calculation. In this case, the specific energy consumption for producing a unit of product was adopted [40], in particular, the thermal energy load required for manufacturing a Parmigiano Reggiano cheese wheel. To achieve this, a survey was conducted with six cheese factories. Between 2022 and 2023, their annual production ranged from 10,000 to nearly 60,000 wheels of Parmigiano Reggiano per year. The average capacity of the analysed cheese factories was 30,000 wheels per year, which was considered a suitable size for the type of investment proposed in this study. Consortium defines "Small cheese factories" as cheese factories where the production of wheels is fewer than 2000 per year [41]. Even if small factories are quite common, the proposed solution is considered more suitable for bigger ones (e.g. 30,000 wheels/year) due to the complexity of installing a hydrogen production, storage and combustion facility. Additionally, another cheese factory, producing 65,000 wheels per year and requiring over 6 GWh of thermal energy annually, was examined but excluded from the analysis. In this specific case, it was not possible to separate the methane consumption for cheese production from that used in the whey processing facility. Only the total methane consumption for both processes was available, making it impossible to allocate a realistic value solely to cheese production. For other two cheese factories, methane was used for the storage and for another whey processing facility. However, in these cases the owner was able to provide an estimate of the quantity of methane used solely for the cheese factory producing Parmigiano Reggiano. To avoid potential overestimation resulting from including heating requirements during the winter period (energy use not directly related to cheese production), the thermal energy consumption was assessed both on a yearly basis and separately for the months between May and September for the years 2022 and 2023. The energy requirements were assessed based on the number of wheels produced, calculating the power needs for each wheel for every cheese factory. When the data referred to the milk processed, the thermal need per kilogram of milk was converted into thermal need per wheel, assuming that one wheel is produced by processing 550 kg of milk [42]. This survey resulted in a thermal energy requirement of 66 ± 6 kWh per Parmigiano Reggiano wheel (6 represents the standard deviation of the sample) when considering the annual average consumption, and 63 ± 10 kWh considering only the warmer months. The survey was considered representative as the six cheese factories analysed have an overall wheel production of approximately 180,000 wheels of cheese. Considering that the overall production of Parmigiano Reggiano cheese is approximately 3 million wheels per year, this was considered a representative sample of medium-large size Parmigiano Reggiano cheese factories [43]. To remain conservative and to avoid over-accounting for other potential thermal users that may be present during production and require methane but are not connected to steam generation, the proposed solution was designed to meet a thermal requirement of 66 kWh per wheel for a cheese factory that produces 30,000 wheels every year. This results in 1.98 GWh per year (5.425 MWh/day).

2.2. Hydrogen utilization strategies

Two distinct hydrogen storage and utilization strategies were designed to meet the thermal energy demands of Parmigiano Reggiano cheese manufacturing: *seasonal* and *daily*.

The primary distinction lies in their operational approach to managing hydrogen availability throughout the year. The *seasonal* strategy aims to balance hydrogen production over the annual cycle, storing surplus generated during high-production periods (e.g., summer) for use during low-production periods (e.g., winter), assuming a constant amount of hydrogen used each day. In contrast, the *daily* strategy addresses short-term fluctuations between hydrogen production and consumption. It operates with a dynamic daily fuel mix where the quantity of hydrogen used is adjusted based on the hydrogen produced the previous day, utilizing the maximum amount available from short-term storage; this includes the immediate use of hydrogen generated during boiler operating hours (e.g., 7:00–9:00 a.m.) with subsequent production stored for the following day. While the production system size is identical for both *seasonal* and *daily* strategies (PV array, electrolyser, and compressor), the operational dynamics significantly influence the required hydrogen storage capacity and configuration. In this study, four different hydrogen volumetric fractions f were considered to meet the thermal energy demand of the process: 0.2 (20 % H_2, 80 % CH_4), 0.5 (50 % H_2, 50 % CH_4), 0.75 (75 % H_2, 25 % CH_4) and 1 (100 % H_2). The interpretation of f differs depending on whether the scenario involves *seasonal* or *daily*, except for the case that relies entirely on hydrogen for thermal energy production ($f = 1$). In this case, there is no distinction between the two strategies, as the system operates solely on hydrogen throughout the year. In the *seasonal* storage strategy, f represents a fixed hydrogen content used in the steam generation process throughout the year. Conversely, in the *daily* storage strategy, the hydrogen fraction varies dynamically on a daily basis. It is calculated as the actual volume of hydrogen used relative to the total fuel consumed over the course of the year. To clarify, an f ratio of 0.2 in the *daily* storage strategy means that 20 % of the total gas volume used for steam production over the entire year was hydrogen. However, this percentage can vary significantly from day to day depending on hydrogen availability. This daily variability reflects the fluctuating availability of solar irradiation, which influences the quantity of hydrogen produced via electrolysis each day. The f ratios used for the evaluation were selected based on existing literature and relevant data [28,30]. An f ratio of equal or lower than 0.2 is not expected to significantly influence the combustion process within steam boilers. At this level, the characteristics of the fuel mixture are primarily governed by methane, which guarantees that the operational efficiency of the boiler is maintained. Furthermore, the release of the UNI/TS 11854 technical standard in 2022, which addresses boilers operating with hydrogen-methane blends up to 20 % hydrogen by volume, facilitates the deployment of such systems, particularly for boilers with a nominal thermal capacity of 300 kW [44]. However, since the thermal power considered in the present study exceeds this value, the applicability of this standard is not further considered. At higher hydrogen concentrations, combustion dynamics may be substantially altered, potentially requiring modifications to the combustion system or the installation of an additional boiler to ensure stable operation [45]. Accordingly, in this study, a single boiler was considered for the *seasonal* scenario where $f = 0.2$, and for $f = 1$. For all other cases, two separate boilers were assumed: one operating exclusively on methane and the other exclusively on hydrogen.

2.3. Photovoltaic system design and simulation

The solar irradiance data refer to a Parmigiano Reggiano production center located in Modena, Italy, which lies in the central province of the Parmigiano Reggiano production zone. The data were obtained from the Photovoltaic Geographical Information System (*PVGIS*) website [46]. *PVGIS* is an online platform that offers complimentary access to solar radiation and temperature datasets, typical meteorological year (*TMY*) information, and tools for evaluating photovoltaic performance across various global locations. Furthermore, *PVGIS* serves as an advanced GIS-based resource that delivers accurate solar radiation predictions and simulations of photovoltaic energy output and numerous studies have employed *PVGIS* models to enhance the dependability of photovoltaic power generation [47,48].

Fig. 1 depicts the total observed solar irradiation values over the course of an entire year for the selected location obtained from the *PVGIS* web page [46]. Direct normal irradiance (*DNI*) is the solar energy received per unit area, measured perpendicular to the sun's rays. Global horizontal irradiance (*GHI*) refers to the cumulative shortwave radiation incident on a horizontal plane at the Earth's surface and Diffuse horizontal irradiance (*DHI*) is the sunlight that reaches a flat surface after being scattered by the atmosphere [49,50].

Using SAM software, the potential energy production for different solar system tilt and azimuth angles in the selected region was determined. The SAM software was created by the National Renewable Energy Laboratory (NREL). SAM's performance models conduct calculations of a power system's electrical output at each timestep, producing a series of timeseries data that reflects the system's electricity generation throughout a year. Using SAM, it is possible to model energy systems such as PV, concentrating solar power (CSP), wind, geothermal power, geothermal co-production, and biomass [51]. A review of the literature revealed that SAM is commonly used for calculating energy production in PV systems [52–54]. Furthermore, the software's availability as a free techno-economic tool was a key factor in its selection for this study.

The simulation methodology involved optimizing the performance of a selected solar panel model, the Panasonic EVPV350K (350W), chosen for its high efficiency and dependability. Initially, a comprehensive parametric analysis was conducted in SAM across various azimuth and tilt angles to identify the optimal configuration for maximum annual energy yield in the specific geographic and climatic conditions. This analysis established that peak energy output (497.05 kWh per panel annually) is achieved at a tilt angle of 39.05° and an azimuth angle of 149.85°. The results of this parametric analysis are demonstrated in Fig. 2.

In addition to the optimal configuration, several other scenarios were simulated to assess performance under practical constraints and common installation practices. These included a tilt angle of 12° (approximately 21.3 %) [55], representing a typical roof angle for cow barns suitable for PV installation, and three azimuth orientations, considering that barns may have various alignments, particularly west, south and east. Therefore, six distinct PV system configurations were evaluated using SAM, representing the following tilt-azimuth pairs: the optimal (39.05°, 149.85°), optimal tilt with south orientation (39.05°, 180°), practical tilt with optimal azimuth (12°, 149.85°), and practical tilt with south, east, and west orientations (12°, 180°; 12°, 90°; 12°, 270°). While the 12° tilt scenarios reflect practical installation feasibility on existing structures, the optimal tilt and azimuth configuration remains compatible with alternatives like static agrivoltaic systems [56,57].

The hourly energy output data simulated by SAM for each of these six PV configurations were subsequently used as the primary input for calculating the hourly, daily, and annual hydrogen production rates via the electrolyser model (described in Section 2.4) and for determining the required sizes of the various system components (electrolyser, compressor, converter, storage) under different operational scenarios.

A systematic, multi-stage optimization methodology was employed to determine the photovoltaic system dimensions for all scenarios. For each hydrogen demand level, the analysis first established a baseline by determining the system size for the single most productive PV configuration (39.05° tilt, 149.85° azimuth). This was achieved through iterative simulations to find the minimum quantity of panels needed to meet that specific annual hydrogen target. The annual electrical energy generated in this baseline case then served as a reference target for that

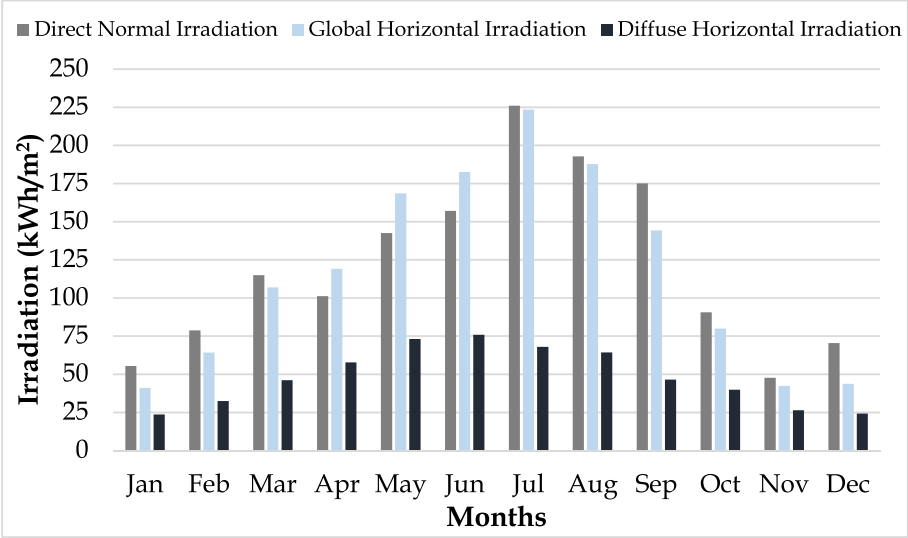

Fig. 1. Monthly total direct normal irradiation, global horizontal irradiation and diffuse horizontal irradiation.

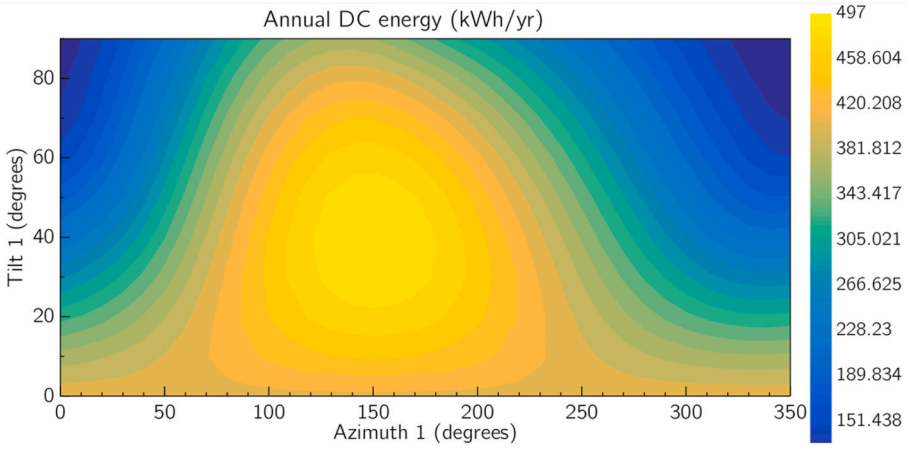

Fig. 2. Annual energy production for different tilt and azimuth angles.

demand group. This energy target was used to make a preliminary calculation of the panel count for the other PV configurations with different tilt and azimuth angles. However, this initial figure was considered tentative due to two constraints: the necessity for an integer number of panels and, more significantly, the electrolyser's variable efficiency. The electrolyser's performance is sensitive to the hourly power delivery pattern, meaning that different system orientations produce varying hydrogen outputs, even with comparable total annual energy. Consequently, each of the other configurations within that demand group underwent a final, detailed refinement. Beginning with the preliminary count, the number of panels was incrementally altered, and a complete annual simulation was conducted for each change. This was done to pinpoint the lowest integer panel count that fulfilled the precise hydrogen production requirement for that specific hydrogen need. By systematically applying this staged methodology across all demand levels, the study ensured an accurately and efficiently sized system for every unique scenario.

The sizing of the DC-DC converter represented a pivotal aspect of the system's design framework. This sizing was dictated by the maximum hourly power output of the PV array, ensuring that the converter could effectively handle peak energy production without encountering bottlenecks or energy losses. By opting for a converter capable of accommodating the highest energy output levels from the PV system, the overall efficiency and reliability of the energy conversion process were significantly enhanced.

2.4. Electrolyser modelling

Electrolysers are electrochemical systems designed to generate hydrogen by means of water electrolysis. In this study, an alkaline electrolyser was selected because it represents the most prevalent technology, owing to its established reliability, affordability, and substantial capacity for hydrogen production [58]. The equations of the chemical reactions for the alkaline electrolyser are given.

$$Anode: 2OH^- \rightarrow \frac{1}{2} O_2 + H_2O + 2e^- \quad (1)$$

$$Cathode: 2H_2O + 2e^- \rightarrow H_2 + 2OH^- \quad (2)$$

$$Overall\ Cell: 2H_2O \rightarrow O_2 + 2H_2 \quad (3)$$

The electrolyser model used in this study is an advanced alkaline device with a maximum power output of 26 kW. It operates at nominal conditions of 7 bar and 80 °C and consists of 21 bipolar cells connected in series, each with an active area of 0.25 m^2. The model has been created based on the mathematical model of Ulleberg [59]. The same model was used in other studies to calculate the H_2 production [60,61]. The cell voltage V_{cell} can be calculated with the following equation [62]:

$$V_{cell} = V_{rev} + V_{ohm} + V_{act} \tag{4}$$

$$V_{ohm} = \frac{r_1 + r_2 T}{A} I \tag{5}$$

$$V_{act} = z \log\left(\frac{t_1 + \frac{t_2}{T} + \frac{t_3}{T^2}}{A} I + 1\right) \tag{6}$$

In these equations, V_{rev} shows the reversible voltage (1.184 V at 80 °C and 1 bar), V_{ohm} is the ohmic losses and V_{act} is the activation losses. Parameters for the current - voltage curve which are r_1, r_2, z, t_1, t_2 and t_3 were determined considering the study of Ulleberg [59]. T is the operating temperature (°C), A is the area of the electrode (m^2) and I shows the electrode current (A). The total hydrogen production from the electrolyser, $\dot{n}_{H_2}$ is:

$$\dot{n}_{H_2} = \eta_F \frac{N_{cell} I}{2F} \tag{7}$$

$$\eta_F = \frac{\left(\frac{I}{A}\right)^2}{f1 + \left(\frac{I}{A}\right)^2} f2 \tag{8}$$

Here, η_F is the faraday efficiency, F is the Faraday constant (96,485 coulombs per mol), N_{cell} is the number of cells in series for one stack, and $f1$ and $f2$ are specific parameters for the modelled electrolyser [59]. The electrolyser model was validated by comparing the measured values [59,63] with the numbers from our model, as shown in Fig. 3.

As stated in earlier sections of this study, the hourly power output from the PV panels was calculated using the SAM software. It is important to highlight that increasing the number of cells arranged in series within an electrolyser generally leads to an increase in its rated power. Each individual cell in an electrolyser operates at a specific voltage, and when connected in series, their voltages are summed, resulting in a higher total voltage for the electrolyser. In designing this system, both the power generated by the PV system and the current through the electrolyser were taken into consideration. Assuming a 95 % efficiency for the DC-DC converter [65,66], power losses between the PV system and the electrolyser, as well as hydrogen production, were calculated using a MATLAB/Simulink model. The sizes of the electrolysers were selected in multiples of 26 kW to ensure operational efficiency and to avert any potential system overload.

2.5. Hydrogen storage and compressor power

It is well-established that low-pressure hydrogen storage requires a significantly larger storage volume. Appropriate pressure storage for industrial application varies from about 30 bar to 1000 bar [67]. In this study, we have calculated the system properties for two different hydrogen storage tank pressure values (S_p): 30 bar and 350 bar. A review of the literature highlights that storing hydrogen at 350 bar is commonly employed due to the cost-effectiveness and widespread use of this method [68,69]. However, for stationary agro-industrial applications, where space constraints are typically less critical, and considering safety factors [70], storage at a lower pressure of 30 bar is also a viable option

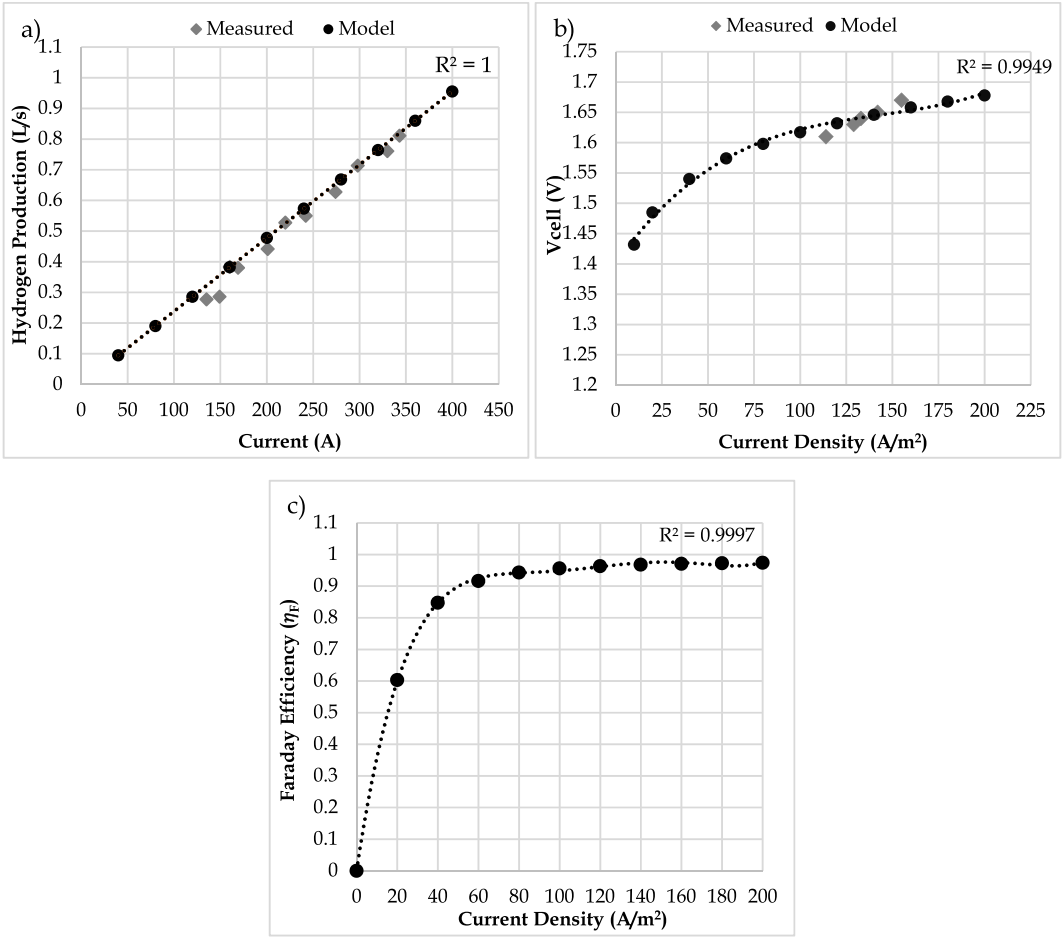

Fig. 3. Comparison between observed [59,64] and calculated values for: a) Hydrogen production, b) Cell voltage and c) Faraday efficiency η_F relative to current density.

and was therefore included in the analysis. The power required for the compressor was calculated using the following equation [71]:

$$p_{comp} = \dot{m} \cdot c_p \cdot \frac{T_h}{\eta_{comp}} \cdot \left[\left(\frac{p_0}{p_i} \right)^{\frac{k-1}{k}} - 1 \right] \quad (9)$$

Here, $\dot{m}$ is the mass flow rate of the hydrogen (kg/s), c_p is the specific heat at constant pressure, T_h is the hydrogen temperature before the compression in kelvin, η_{comp} is the compressor efficiency, p_0 is the inlet pressure and p_i is the outlet pressure of the hydrogen and k is the ratio of hydrogen specific heats (assumed constant). k and c_p were taken as 1.4 and 14.4 kJ/(kg K), respectively. The compressor efficiency was assumed to 75 % [72] and the p_0 and T_h values were defined according to the modelled electrolyser [59].

Furthermore, the power of the compressor was entirely provided by the PV system, indicating that there were no supplementary energy requirements for compressor operation. Analysis reveals that approximately 2 % and 7 % of the total power output from the PV system must be allocated to the compressors for storage pressures of 30 bar and 350 bar, respectively (see Eq. (9)). This allocation further underscores the self-sufficiency and efficiency of the proposed system design.

2.6. Hydrogen demand

A literature review indicates that low-capacity boilers (0.1–4 MW) generally achieve efficiencies between 90 % and 92 % [73]. Previous studies on H_2–CH_4 mixtures have reported boiler efficiencies of up to 92 % [28,30]. However, for f ratios higher than 0.2, the installation of two boilers was considered: one operating 100 % on methane and the other operating 100 % on hydrogen. In this study, the boiler efficiency is assumed to be 92 % for systems operating on a single type of fuel, either pure methane or pure hydrogen. In contrast, for the co-firing configuration involving a 20 % hydrogen–methane mixture (corresponding to the seasonal storage case with $f = 0.2$), a slightly lower efficiency value of 90 % is considered. This reduction reflects possible performance losses when a boiler originally optimized for natural gas is used with a blended fuel composition. Such a conservative assumption aligns with observations in previous studies. For example, Boulahlib et al. [33] experimentally demonstrated that thermal efficiency tends to decline as the hydrogen content in the mixture increases. Likewise, Wang et al. [28] reported that industrial boilers not fully optimized for hydrogen-rich fuels exhibit efficiency drops as the hydrogen share rises. Although several studies indicate that introducing up to 20 % hydrogen does not significantly impact boiler integrity or component wear, a minor decrease in operational efficiency remains plausible [45]. Therefore, adopting a 2 % efficiency reduction for this co-firing case provides a reasonable and literature-supported estimation.

The properties of H_2 and CH_4 used were taken from Ref. [27]. To ensure a consistent basis for thermodynamic calculations, the volumetric fraction (f) was first converted to a mass fraction (ω_{H_2}) for each fuel blend scenario. The mass fraction of hydrogen is given by:

$$\omega_{H_2} = \frac{f \cdot \rho_{H_2}}{f \cdot \rho_{H_2} + (1-f) \cdot \rho_{CH_4}} \quad (10)$$

$$\omega_{CH_4} = 1 - \omega_{H_2} \quad (11)$$

$$\rho_{mixture} = f \cdot \rho_{H_2} + (1-f) \cdot \rho_{CH_4} \quad (12)$$

Subsequently, the mass-based Higher Heating Value ($HHV_{mixture}$) of the fuel blend was determined using a mass-weighted average of the individual fuel components:

$$HHV_{mixture}(kWh/kg) = (\omega_{H_2} \cdot HHV_{H_2}) + (\omega_{CH_4} \cdot HHV_{CH_4}) \quad (13)$$

The properties of the pure fuels and the calculated properties for the mixtures are shown in Table 1.

Table 1
Properties of Hydrogen, Methane and their mixtures [27].

	H_2	CH_4	$f = 0.2$	$f = 0.5$	$f = 0.75$	$f = 1$
ω_{H_2}	1	0	0.03038	0.11139	0.27328	1
ω_{CH_4}	0	1	0.96962	0.88861	0.72672	0
ρ [kg/m^3]	0.09	0.718	0.5924	0.404	0.247	0.09
HHV [kWh/kg]	39.35	15.405	16.133	18.07274	21.94951	39.35185

The following formula was used to calculate the required quantities of H_2 and CH_4 to meet the energy demand of the boiler [74]:

$$m_{fuel} = Q_{fuel} \,/\, HHV_{fuel} \quad (14)$$

Here, m_{fuel} shows the required fuel mass in kg, Q_{fuel} is the heat demand (kWh) and HHV_{fuel} is the higher heating value of the fuel mixture (kWh/kg).

The objective was to meet the boiler's thermal energy demand (1.98 GWh) using a combination of hydrogen and methane. Table 2 presents the annual hydrogen demand required to satisfy this thermal load for the four f ratios considered. In contrast, the estimated annual methane consumption needed to meet the full 1.98 GWh energy demand using only methane would be approximately 128,526 kg.

2.7. CO_2 savings and Nox emissions

The reduction in CO_2 emissions was estimated based on the avoided methane consumption, multiplied by its global warming potential (GWP). Although methane combustion primarily produces CO_2 and H_2O, additional factors must be considered, such as methane leakages from oil and gas operations. The emission metrics provided by *IPCC* indicates that CH_4 has a radiative forcing 29.8 times greater than CO_2 over a 100-year horizon (GWP_{100}) and 82.5 times greater over a 20-year horizon (GWP_{20}). Methane also acts as a precursor to tropospheric ozone (O_3) [69,75]. For these reasons, the avoided CO_2 emissions cannot be approximated solely by the 2.75 kg of CO_2 released per kg of CH_4 burned [76]. Following the Guidelines provided by *IPCC*, a value of 3.11 kg of CO_2 released per kg of CH_4 burned were used for the economic assessment. Details regarding the chosen values are provided in Appendix C.

This techno-economic study did not include a predictive model for NOx emissions, as there is still no clear consensus in the literature on how hydrogen addition influences them [34]. The effect of hydrogen enrichment on NOx formation is quite complex, involving a balance between competing physical processes. On one hand, introducing hydrogen can intensify NOx generation by raising combustion temperatures and increasing reactive radicals such as OH, H, and O that facilitate thermal NO formation. On the other hand, hydrogen's combustion characteristics allow for stable flame operation even at higher excess air ratios. Operating under these leaner conditions can lower the flame temperature sufficiently to counteract the mechanisms that promote NOx formation, potentially leading to an overall reduction in emissions [27].

2.8. Economic assessment

The economic model proposed to analyze the full-scale investment consists of the initial investment and maintenance costs of all

Table 2
Properties of the fuel mixture, H_2 and CH_4 need in kg.

	$f = 0.2$	$f = 0.5$	$f = 0.75$	$f = 1$
H_2 need in kg/year	3729.12	12,203.2	24,651.7	50,315.3
CH_4 need in kg/year	119,000	97,354.1	65,555.3	0

components, components' amortization and degradation with residual values, and benefits from cost-savings from the reduced methane needed. The output of the economic analysis is the Net Present Value (*NPV*) of the investment, expressed as the difference between net present benefits (methane savings) and net present costs (installation and maintenance costs). In this analysis, a Monte Carlo simulation approach is employed, assuming that a given set of input parameters is randomly generated from predefined probability distributions. The Monte Carlo simulation method is widely adopted to investigate the behavior of deterministic models when the main input parameters are allowed to vary according to specified probability distributions [77]. The following section describes the input variables and the corresponding probability distributions adopted for the simulation. A total of 10,000 model replications were performed to obtain the final outputs of the analysis. A sensitivity analysis on parameters and full discussion of all main assumptions of the model were also provided. A time horizon of 15 years was assumed.

2.8.1. Component costs and residual value

Components fixed costs include the compressor, the electrolyser, the converter, the PV panels, the Storage unit, and the additional boiler needed (only for certain scenarios, as explained in previous sections). The *CAPEX* for compressor, electrolyser and converter, are reported in Table 3, *Panel a*, while for the boiler, since it is scenario-specific, it is reported in Table B1. Moreover, we consider for each component yearly maintenance costs to be paid from year 1 to year 15, scaling with inflation. The maintenance cost is assumed to be 2 % of the initial *CAPEX* [21,78]. The cost for PV panels and storage are considered as an input of the Monte Carlo simulation (Table 3, *Panel b*). For those parameters, we assume uniform distribution between, respectively 550 €/kW and 800 €/kW for the PV panels and 75 €/kg and 150 €/kg for the storage. The maintenance (*O&M*) costs for these two parameters will be, for each simulation, the 2 % of the sampled cost. In other words, for each replication of the model, the *O&M* percentage on the *CAPEX* is constant.

The time horizon of the project, 15 years, matches the minimum lifetime among components, which is the one of the converter [85,86]. For the other components, it is assumed a life-span of 25 years, and a residual value at year 15 which should be interpreted as the value generated by the asset after the end of the project lifetime, by selling or by employing it in other projects. The residual value of component c (RV_c) is computed using a linear depreciation method:

$$RV_c = \frac{RL_c}{TL_c} \cdot CAPEX_c \tag{15}$$

Where RL_c and TL_c are the residual life and the total life of the component c, respectively. The net present value of all costs was computed by summing the *CAPEX* with the *O&M* costs and the residual value of all components, specifically discounted to take into account the time value of money.

Table 3
Cost considered for the economic analysis.

	CAPEX	*O&M*	Life time	Inflation rate
Panel a				
Compressor	7250 €/kW [79,80]	145 €/kW	25 years [81]	1.50 %
Electrolyser	750 €/kW [80,82]	15 €/kW	25 years [82,83]	1.50 %
Converter	85 €/kW [84–86]	1.7 €/kW	15 years [85,86]	1.50 %
Panel b	**Distribution**			
PV panels	Uniform (550 €/kW,800 €/kW) [87,88]	2 % of the simulated cost	25 years [20,86,89]	1.50 %
Storage	Uniform (75 €/kg,150 €/kg) [90]	2 % of the simulated cost	25 years [20,89]	1.50 %

Note: This table provides the main fixed capital costs for the economic assessment, as well as the inflation rate and the O&M costs considered. Some values have been readapted from the displayed references to ensure consistency with the context and the objectives of this study.

For hydrogen energy projects, discount rate typically fall in the range between 2 % and 15 % (e.g., see Refs. [91–94]). In this work, a discount rate of 4 % was assumed to highlight potential benefit in the long term of energy and green projects, while large discount rates tend to discourage investment that have positive return in the longer term. A sensitivity on this value was also provided in the range of 3 %–8 %.

The final Net Present Total Costs (*NPTC*) is a function of the PV tilt and azimuth, the storage pressure S_p and the f ratio used, and it is computed as follows:

$$NPTC = \sum_c CAPEX_c + \sum_c \sum_{t=1}^{15} \frac{OPEX_{c,t}(1+\nu_c)^t}{(1+\delta)^t} - \frac{RV_c}{(1+\delta)^{15}} \tag{16}$$

Where ν and δ are the inflation rate and the discount rate, respectively.

2.8.2. Methane savings

The methane savings from its substitution with hydrogen were included in the economic assessment for each scenario (Table B1), for both *daily* storage and *seasonal* storage. The prices and inflation rate considered in this analysis represent a balance between insights from previous academic research and real-world market trends. Notably, methane prices can experience significant fluctuations due to geopolitical factors. To account for these uncertainties, data from the Eurostat database of Natural gas price statistics database [95] were used to consider fluctuations of this parameter, focusing on non-household consumers. These data are provided in €/kWh and were converted to €/kg by dividing by the methane higher heating value (HHV) reported in Table 1. Henceforth, the natural gas price was adopted as an input for the Monte Carlo simulation, assuming uniform distribution between its maximum and minimum level in Italy between 2021 and 2022-s1. 2022-s2, 2023 and 2024 were excluded since there was a huge spike variations that might distort the analysis. As a matter of fact, 2022-s2 are three times higher than 2021-s1 data, while 2023-s2 and 2024-s1 data are both lower than 2022-s1. For *daily* storage, a uniform distribution between 0.4636 €/kg and 0.6932 €/kg was used for the summer period, and a between 0.6932 €/kg and 0.9226 €/kg for the winter period. For the *seasonal* storage, a uniform distribution between 0.4636 €/kg and 0.9226 €/kg was applied. The assumed inflation rate for methane is 3 %, for which a sensitivity analysis was provided. The Net Present Benefit (*NPB*) from methane savings was computed by simply discounting each year savings:

$$NPB = \sum_{t=1}^{15} \frac{MS(1+\nu_{CH_4})^t}{(1+\delta)^t} \tag{17}$$

Where ν_{CH_4} represent the methane inflation rate, and thus $MS(1+\nu_{CH_4})^t$ is the annual positive cashflow from saving methane.

The main variable of interest considered to perform the economic assessment was the Net Present Value. From the *NPTC* and the *NPB*, it is possible to derive the *NPV* of the investment, as the difference between the two values in eqs. (16) and (17);

$$NPV = \sum_{t=1}^{15} \frac{MS(1+\nu_{CH_4})^t}{(1+\delta)^t} - \left[\sum_c CAPEX_c + \sum_c \sum_{t=1}^{15} \frac{OPEX_{c,t}(1+\nu_c)^t}{(1+\delta)^t} - \sum_c \frac{RV_c}{(1+\delta)^{15}} \right] \tag{18}$$

Given the model's assumptions, the *NPV* will be negative in nearly all scenarios. Therefore, it should not be viewed in isolation but rather in the context of a cleaner production and of the investment impact on reducing *GHG* emissions by lowering methane usage. Henceforth, as an

additional result aimed to analyze the potential public support for the green transition (in the form of a grant that covers a part of the initial capital cost), we compute the minimum Public Funding Rate (*PFR*) for each scenario. The minimum *PFR* was defined as the value that sets the Net Present Value of the investment equal to zero. Therefore, the *PFR* is computed as follows:

$$\sum_{t=1}^{15}\frac{MS(1+\nu_{CH_4})^t}{(1+\delta)^t}-\left[(1-PFR)\sum_c CAPEX_c+\sum_c\sum_{t=1}^{15}\frac{OPEX_{c,t}(1+\nu_c)^t}{(1+\delta)^t}-\frac{RV_c}{(1+\delta)^{15}}\right]=0 \tag{19}$$

The minimum *PFR* is crucial as it provides a benchmark for understanding how public support can help enterprises in the green transition by reducing the financial burden of sustainable investments on their operations. Specifically, a minimum *PFR* of 40 % indicates that if public grants cover 40 % of the initial *CAPEX*, the investment in the green transition reaches the break-even point.

Lastly, to assess cost-effectiveness, in relation to the public support, we calculate the ratio between saved CO_{2eq} emission and the public funding that can support the investment at zero *NPV*. This variable, that can be defined as Emissions Saved per euro of Public Support (*ESPS*) is measured in $kgCO_{2eq}/€$, and it can be read as an eco-cost indicator, and it is computed as follows:

$$ESPS=\frac{CO_{2eq\ savings}}{PFR\cdot CAPEX_c} \tag{20}$$

The denominator is the amount of money from public support that reduces the burden of the investment to the singular entrepreneur so that the *NPV* is zero. Thus, this indicator could be interpreted as an indicator of efficiency of public spending into the green transition: the higher the *ESPS*, the higher the reduction of CO_{2eq} emission per euro of public funding support invested.

Table 4
Component sizing for the various scenarios.

No	Tilt	Azimuth	S_p, [bar]	f	P_{PV}, [kW]	P_{el}, [kW]	P_{conv}, [kW]	P_{comp}, [kW]	$P_{b,H_2,d}$ [kW]	$P_{b,H_2,s}$ [kW]	$S_{m,d}$, [kg]	$S_{v,d}$, [m^3]	$S_{m,s}$, [kg]	$S_{v,s}$, [m^3]
1	39.05°	149.85°	350	0.20	157.85	130	148	8.5	638	–	14.98	0.64	582.8	24.9
2	39.05°	149.85°	30	0.20	149.8	130	140	2.26	638	–	14.98	6.24	582.9	242.71
3	39.05°	180°	350	0.20	163.45	130	151.7	8.75	661	–	16.17	0.69	556.6	23.78
4	39.05°	180°	30	0.20	155.05	130	143.8	2.32	661	–	16.16	6.73	555.6	231.34
5	12°	149.85°	350	0.20	172.2	130	149.5	8.61	725	–	17.21	0.74	737.3	31.5
6	12°	149.85°	30	0.20	163.45	130	142	2.3	725	–	17.22	7.17	737.8	307.2
7	12°	180°	350	0.20	174.65	130	152	8.75	731	–	17.59	0.75	728.3	31.12
8	12°	180°	30	0.20	165.9	130	144.5	2.33	731	–	17.60	7.33	730.8	304.3
9	12°	90°	350	0.20	182.7	130	154	8.84	757	–	17.72	0.76	822.8	35.15
10	12°	90°	30	0.20	173.25	130	145.5	2.35	757	–	17.71	7.37	820.8	341.76
11	12°	270°	350	0.20	201.6	156	161.4	9.42	816	–	19.96	0.85	838.3	35.82
12	12°	270°	30	0.20	191.1	156	153	2.5	816	–	19.94	8.30	835.3	347.8
13	39.05°	149.85°	350	0.5	513.45	442	479	27.9	2084	660	49.00	2.09	1897.9	81.09
14	39.05°	149.85°	30	0.5	490.35	416	457.3	7.38	2082	660	48.94	20.38	1893.1	788.24
15	39.05°	180°	350	0.5	532.35	442	494	28.6	2159	660	52.87	2.26	1810.7	77.36
16	39.05°	180°	30	0.5	507.85	416	471	7.58	2156	660	52.83	22.00	1809.0	753.22
17	12°	149.85°	350	0.5	560	442	485	28.2	2365	660	56.28	2.40	2401.3	102.59
18	12°	149.85°	30	0.5	532.35	442	461.35	7.48	2367	660	56.30	23.44	2403.7	1000.83
19	12°	180°	350	0.5	568.4	442	495	28.7	2386	660	57.55	2.46	2378.6	101.62
20	12°	180°	30	0.5	542.85	416	472.5	7.6	2385	660	57.48	23.93	2373.6	988.31
21	12°	90°	350	0.5	594.3	442	499	28.9	2472	660	57.95	2.48	2683.5	114.65
22	12°	90°	30	0.5	564.55	442	474	7.66	2472	660	57.93	24.12	2679.7	1115.74
23	12°	270°	350	0.5	662.9	468	531	30.72	2667	660	65.16	2.78	2731.5	116.70
24	12°	270°	30	0.5	630	468	504.35	8.15	2667	660	65.16	27.13	2731.6	1137.36
25	39.05°	149.85°	350	0.75	1040.55	858	970.5	56.2	2712	1330	98.90	4.23	3827.8	163.54
26	39.05°	149.85°	30	0.75	991.55	832	925	14.9	2712	1330	98.86	41.16	3825.7	1592.93
27	39.05°	180°	350	0.75	1079.05	858	1001	57.7	2712	1330	106.74	4.56	3654.7	156.14
28	39.05°	180°	30	0.75	1026.9	832	952	15.3	2712	1330	106.70	44.43	3655.1	1521.90
29	12°	149.85°	350	0.75	1135.4	858	984	56.9	2712	1330	113.66	4.86	4851.9	207.29
30	12°	149.85°	30	0.75	1081.85	832	937.6	15.1	2712	1330	113.61	47.30	4848.0	2018.57
31	12°	180°	350	0.75	1149.05	884	1000	57.9	2712	1330	116.22	4.97	4802.0	205.16
32	12°	180°	30	0.75	1092	884	950.35	15.36	2712	1330	116.21	48.39	4801.8	1999.33
33	12°	90°	350	0.75	1201.2	884	1008	58.3	2712	1330	117.02	5.00	5414.6	231.33
34	12°	90°	30	0.75	1144.5	858	960.75	15.45	2712	1330	116.98	48.71	5411.7	2253.29
35	12°	270°	350	0.75	1340.15	936	1072.9	62	2712	1330	133.98	5.72	5515.6	235.65
36	12°	270°	30	0.75	1276.8	910	1022.15	16.5	2712	1330	133.89	55.75	5514.6	2296.15
37	39.05°	149.85°	350	1	2130.45	1716	1987	114.63	2712	2712	7806.5	333.53	7806.5	333.53
38	39.05°	149.85°	30	1	2021.6	1716	1885	30.41	2712	2712	7804.0	3249.42	7804.0	3249.42
39	39.05°	180°	350	1	2203.6	1742	2044.2	117.8	2712	2712	7461.7	318.80	7461.7	318.80
40	39.05°	180°	30	1	2090.9	1742	1940	31.24	2712	2712	7457.4	3105.11	7457.4	3105.11
41	12°	149.85°	350	1	2324.35	1716	2014.3	116.0	2712	2712	9891.5	422.61	9891.5	422.61
42	12°	149.85°	30	1	2206.05	1716	1912	30.8	2712	2712	9896.0	4120.49	9896.0	4120.49
43	12°	180°	350	1	2355.5	1742	2050	118.0	2712	2712	9790.7	418.307	9790.7	418.307
44	12°	180°	30	1	2235.45	1742	1945	31.3	2712	2712	9792.7	4077.48	9792.7	4077.48
45	12°	90°	350	1	2462.6	1742	2068	119.0	2712	2712	11,043.0	471.81	11,043.0	471.81
46	12°	90°	30	1	2333.45	1742	1962	31.56	2712	2712	11,043.0	4598.08	11,043.0	4598.08
47	12°	270°	350	1	2744	1872	2197	126.6	2712	2712	11,253.4	480.80	11,253.4	480.80
48	12°	270°	30	1	2604	1872	1872	33.57	2712	2712	11,253.4	4685.7	11,253.4	4685.7

3. Results and discussion

3.1. Component sizing

System sizing for key components and an economic analysis were conducted for both storage approaches to evaluate their feasibility. Table 4 illustrates the necessary system properties corresponding to different values of f, S_p, and PV system azimuth and tilt angles for the *seasonal* and *daily* storage. In this table, $S_{m,d}$ and $S_{v,d}$ denote the storage size (kg) and volume for *daily* storage, while $S_{m,s}$ and $S_{v,s}$ refer to the *seasonal* storage scenario. Similarly, boiler sizes (P_b) are denoted with subscripts indicating the fuel and the storage strategy (*d* for *daily*, *s* for *seasonal*).

In addition to the hydrogen production and storage components, the sizing of the steam boiler(s) required to meet the constant thermal demand of the facility was determined. Following the approach outlined in Section 2.2, a single boiler capable of handling H_2–CH_4 blends is assumed for $f = 0.2$ in the *seasonal* storage scenario, thus requiring no new hydrogen boiler ($P_{b,H_2,s} = 0$ for the $f = 0.2$). In the case of $f = 1$, even if only a single boiler is in operation, the purchase of a new boiler capable of operating with 100 % hydrogen is considered. For all other cases, a dual-boiler system is considered, comprising one boiler operating solely on methane ($P_{b,CH4}$) and another operating solely on hydrogen P_{b,H_2}. The sizing logic differs significantly between *daily* and *seasonal* storage strategies due to operational dynamics.

For *daily* storage, the methane boiler size $P_{b,CH_4,d}$ was set to the maximum required capacity (2712 kW) for all *daily* scenarios. This conservative approach ensures that the entire thermal demand can be met by methane during potential consecutive days of low/no hydrogen production or availability. Similarly, for the hydrogen boiler in the *daily* scenario ($P_{b,H_2,d}$), sizes for $f = 0.75$ and $f = 1$ are based on the boiler being able to handle the full thermal load independently. This accounts for potential periods, particularly during summer, where the system might operate entirely on hydrogen for several days. The minimum calculated $P_{b,H_2,d}$ was 638 kW (observed in scenarios 1 and 2).

In the *seasonal* strategy, where daily consumption rates of H_2 and CH_4 are assumed to be constant for a given f, the required boiler sizes ($P_{b,H_2,s}$ and $P_{b,CH_4,s}$) take on a fixed value for each f ratio ($P_{b,H2,s} = 0$ for $f = 0.2$). The required methane boiler sizes ($P_{b,CH_4,s}$) for $f = 0.2$, 0.5, 0.75, and 1.0 correspond to values 2712 kW, 2052 kW, 1382 kW, and 0 (no methane boiler), respectively.

The component sizing for hydrogen production varies significantly based on the selected storage and utilization strategy, f and S_p. As expected, the amount of hydrogen to be produced increases with rising f, necessitating larger and more powerful system components. For instance, at $f = 1$, nearly 13.5 times more hydrogen is required compared to $f = 0.2$ (see Table 2), leading to substantial increases in the number of PV panels (N_{PV}), power demands from the electrolyser (P_{el}), and storage capacities (S_V and S_m).

This scaling effect is clearly reflected in system sizing. The maximum N_{PV} is required for the scenario with an azimuth angle of 270°, a tilt of 12°, an f ratio of 1.0, and an S_p of 350 bar, where 7840 PV panels are necessary to meet hydrogen production demands. Correspondingly, the photovoltaic power output (P_{PV}) reaches its maximum value of 2744 kW in this same configuration. Conversely, the minimum N_{PV}, only 428 panels, and P_{PV} of 149.8 kW are observed for f = 0.2, with an azimuth of 149.85°, a tilt of 39.05°, and an S_p of 30 bar.

The tilt and azimuth angles of the PV system also play critical roles in determining energy yield and component sizing. A 39.05° tilt consistently results in higher instantaneous energy outputs compared to a 12° tilt, thus enabling smaller component sizes for equivalent hydrogen output. This is due to increased solar irradiance capture at steeper angles in the selected region. However, while 39.05° is optimal for energy capture, the 12° tilt remains a practical solution for certain applications, such as installations on agricultural rooftops, where structural constraints limit tilt flexibility. The maximum electrolyser power (P_{el}) of 1872 kW occurs at $f = 1$, with an azimuth of 270° and a tilt of 12°, under both 30 bar and 350 bar storage conditions. This high power demand reflects the substantial energy input required to produce larger hydrogen quantities. The electrolyser HHV efficiency (η_{el}) remains relatively stable across all scenarios, ranging from 74.00 % (Scenario 28) to 75.38 % (Scenario 12), values in line with literature [96]. This relatively stable efficiency, coupled with the increasing power demand (P_{el}) as f grows, suggests that while the electrolyser technology is well optimized, scaling up hydrogen production requires substantial increases in energy input, further reinforcing the need for efficient energy generation and storage strategies.

Compressor and converter power (P_{comp} and P_{conv}) also increase with f, azimuth, and tilt adjustments. The maximum P_{comp}, 126.6 kW, is recorded at $f = 1$, azimuth 270°, tilt 12°, and $S_p = 350$ bar, compared to just 9.42 kW for $f = 0.2$ under the same azimuth, tilt and pressure conditions. The minimum P_{comp}, just 2.26 kW, is observed for $f = 0.2$ with an azimuth of 149.85°, a 39.05° tilt, and 30 bar storage. This wide variation reflects the impact of both hydrogen volume and compression pressure. P_{conv} follows a similar pattern. The maximum P_{conv}, 2197 kW, is required under the same extreme scenario as the maximum N_{PV}, $f = 1$, azimuth 270°, tilt 12°, and $S_p = 350$ bar. The minimum, just 140 kW, is required at $f = 0.2$, azimuth 149.85°, tilt 39.05°, and 30 bar storage, corresponding to the lowest PV power output and hydrogen demand.

Hydrogen storage capacity also reflects the interplay of f, storage pressure and utilization strategies (*daily* and *seasonal*). At lower pressure (30 bar), the volumetric storage requirement (S_V) increases substantially due to hydrogen's lower density. For instance, at $f = 0.2$, tilt 39.05°, and azimuth 149.85° and *seasonal* storage, $S_{V,s}$ is 242.71 m^3 at 30 bar but only 24.9 m^3 at 350 bar, a tenfold reduction. The maximum S_V, 4685.7 m^3, is observed at $f = 1$, 30 bar pressure, 12° tilt, and 270° azimuth, for both *daily* and *seasonal* scenarios.

In contrast, the smallest required S_V, just 0.64 m^3, is found for $f = 0.2$, a tilt of 39.05°, an azimuth of 180°, and 350 bar and *daily* storage. This dramatic difference in storage volumes highlights the critical importance of selecting appropriate pressure levels, as lower-pressure systems may incur higher spatial and infrastructure costs.

In terms of mass-based storage, the maximum S_m (11,253.4 kg) also occurs at $f = 1$, 12° tilt, and 270° azimuth for both 30 bar and 350 bar and *daily* and *seasonal* configurations. The minimum value, $S_m = 14.98$ kg, is found for the *daily* storage scenario at $f = 0.2$, 39.05° tilt, and 149.85° azimuth. These mass storage values further underscore the scalability of the system, with significantly higher hydrogen storage requirements for increased f ratios.

Overall, the component sizing results clearly illustrate that increasing hydrogen production (via higher f ratios) requires a corresponding upscaling of nearly every system parameter, from PV panel count and power ratings to compression and storage infrastructure. The difference between *seasonal* and *daily* storage strategies lies, in most scenarios, primarily in a higher storage capacity for *seasonal*, and a higher hydrogen boiler capacity for *daily*. Conversely, the sizes of the PV system, converter, compressor, and electrolyser determined for *daily* storage are equivalent to those for *seasonal* storage, provided that the f ratio, azimuth angle, tilt angle, and storage pressure remain constant.

This equivalence arises from the fact that the annual hydrogen production is consistent across both scenarios, leading to the sizing of system components being based on this uniform annual production volume. For *seasonal* storage, the system was assumed to commence operations on the 71st day of the year (March 12), a timing that effectively reduces storage requirements. From this day onward, the cumulative net hydrogen, calculated as the difference between hydrogen production and consumption, remains consistently above zero. This approach negates the necessity for external hydrogen supplementation and guarantees that the minimum storage capacity required to fulfil the system's demands is attained. In the context of *daily* storage, operations do not

formally commence on the 71st day. However, for the f ratio equals to 1.0, a similar trend is observed: from this day onward, cumulative hydrogen continues to increase without any reduction. Thus, the hydrogen storage requirements for both *daily* and *seasonal* storage scenarios align, since the surplus hydrogen produced after the 71st day is stored in both instances.

3.2. Economic results

This section presents the results of the economic assessment described in section 2.8. Table 5 summarizes the results of the *NPV*, minimum *PFR* and *ESPS* for each methane/hydrogen fraction in the scenarios, (i.e. 20 %, 50 %, 75 % and 100 %), for both *daily* and *seasonal* storage. The table shows the minimum, average and maximum *NPV*, average minimum *PFR* and average *ESPS* for *seasonal* storage (*Panel A*), for *daily* storage (*Panel B*), for $f = 1$ (*Panel C*) and the difference in absolute terms between *seasonal* and *daily* (*Panel D*). It also provided a reference for the best scenario, defined as the one that most frequently appears as optimal across the Monte Carlo simulation replications. The numbers in parentheses indicate the second-best scenario, observed in cases where a different scenario emerges as optimal in some replications.

As expected, the *NPV* for all scenarios is quite negative, due to the fact that the only positive cash flow in the investment is related to the methane savings, which cannot fully cover all the *NPV* costs. Specifically, within the *CAPEX*, the main source of costs are the fixed costs of the PV systems and the electrolizer, which together account for between 50 % of the total *CAPEX* of the investment. As a result, the methane savings over the 15-year horizon cover only a small fraction of the total *NPV* of the investment. The highest *NPV* (the less negative one), for each f, is found with a PV tilt of 39.05°, a PV azimuth of 149.05° and a S_p of 30 bar, with only few exceptions (less than 10 times over 10,000 replications) for the seasonal storage model. This combination always ensures the lowest *CAPEX*, regardless of the methane/hydrogen combination used. In addition, the lowest *NPV* is always obtained for combinations of PV tilt, PV azimuth and S_p of 12°, 270° and 350 bar respectively.

As the methane savings cover only a small part of the net present costs for both *daily* and *seasonal* storage, the average minimum public funding rate for all scenarios is around 70 %. This means that public support in the form of a subsidy would have to cover at least the 70 % of the initial investment in order to match the net present revenue and net present cost. In this way, public support could reduce the burden on the entrepreneur for this sustainable investment. In terms of emission savings calculated over a 15-year time horizon, this results in an average *ESPS* of between 1.58 and 2.14 $kgCO_{2eq}/€$ across the various scenarios. This means that for every euro of public support received, the investment leads to a reduction in emissions of between 1.58 and 2.14 kg of CO_{2eq}. The amount of CO_2 saved in every scenarios is provided in Table B1.

The comparison between *daily* and *seasonal* storage gives interesting results. When the hydrogen proportion is 20 %, the difference between the two cases is minimal, with an average value of €4532.27 in favour of *seasonal* storage. This means that there is no significant difference in terms of economic investment between the two cases when the hydrogen content is low. On the other hand, when the hydrogen fraction increases (i.e. $f = 0.5$ or $f = 0.75$), the difference between *seasonal* and *daily* storage becomes significant, reaching between 25 % and 30 % of the average *NPV*s in favour of *daily* storage. We can therefore conclude that when the proportion of hydrogen is limited, *daily* and *seasonal* storage have a similar economic evaluation. On the other hand, when the hydrogen content is high, *daily* storage is the most economically viable option.

3.2.1. Sensitivity tests

To corroborate the results of the main analysis, a sensitivity analysis based on the main parameters considered was provided. While the Monte Carlo simulation method offers solid support for the estimated parameters given the assumed distributional specifications, the methane inflation rate and the discount factor were considered as fixed parameters without associated distributions. As a result, potential uncertainty associated with these parameters was not captured by the previous analysis, which could alter the outcome of the economic assessment.

Firstly, the analysis focuses on the methane inflation, as energy and raw material prices and inflation could be highly volatile. This approach aims to consider higher fluctuations of methane prices, as energy prices and inflation are highly volatile for various reasons, such as macroeconomic context and geopolitical factors, market factor and public investments, energy policies [97]. Subsequently, a sensitivity analysis is conducted on the discount rate, which represents the time value of money and can be interpreted as the required rate of return of the potential investors/entrepreneurs in the project.

The sensitivity analysis is provided by repeating the Monte Carlo simulation using the same distributional function as in the main analysis

Table 5
Results of the economic assessment.

Panel A: Seasonal storage						
f	**Min *NPV***	**Average *NPV***	**Max *NPV***	**Average Min *PFR***	**Average *ESPS***	**Best scenario**
0.2	−285,265.41 €	−213,265.26 €	−144,237.28 €	71.74 %	1.72 $kgCO_{2eq}/€$	2 (4)
0.5	−980,838.75 €	−750,748.50 €	−530,018.88 €	73.77 %	1.58 $kgCO_{2eq}/€$	14 (16)
0.75	−1,929,931.50 €	−1,464,942.73 €	−1,018,867.06 €	73.04 %	1.63 $kgCO_{2eq}/€$	26 (28)
Panel B: *Daily* storage						
f	**Min *NPV***	**Average *NPV***	**Max *NPV***	**Average Min *PFR***	**Average *ESPS***	**Best scenario**
0.2	−251,486.47 €	−217,797.53 €	−184,555.11 €	73.81 %	1.71 $kgCO_{2eq}/€$	2
0.5	−711,122.94 €	−600,938.75 €	−492,212.22 €	70.17 %	1.95 $kgCO_{2eq}/€$	14
0.75	−1,330,787.75 €	−1,108,072.07 €	−888,300.19 €	68.10 %	2.14 $kgCO_{2eq}/€$	26
Panel C						
f	**Min *NPV***	**Average *NPV***	**Max *NPV***	**Average Min *PFR***	**Average *ESPS***	**Best scenario**
1	−3,632,805.50 €	−2,948,772.72 €	−2,274,879.00 €	72.82 %	1.65 $kgCO_{2eq}/€$	38
Panel D: Comparison (Seasonal - Daily)						
f	**Min *NPV* diff.**	**Average *NPV* diff**	**Max *NPV* diff**	**Average Min *PFR* diff**	**Average *ESPS* diff**	
0.2	−33,778.94 €	4532.27 €	40,317.83 €	−2.07 %	0.01 $kgCO_{2eq}/€$	
0.5	−269,715.81 €	−149,809.75 €	−37,806.66 €	3.60 %	−0.37 $kgCO_{2eq}/€$	
0.75	−599,143.75 €	−356,870.66 €	−130,566.87 €	4.94 %	−0.51 $kgCO_{2eq}/€$	

and replicating each 10,000 replication on a different value of either the methane inflation rate or the discount rate. For the inflation rate, we chose an interval between 2.5 % and 10 %, while for the discount rate we chose a range between 3 % and 8 %. For both ranges, the sensitivity analysis uses a grid of 100 values. So, for example, it is replicated the full analysis using the previous Monte Carlo approach for the methane inflation rate in the grid between (2.5 %; 2.58 %; 2.65 %; …; 9.93 %; 100 %).

The results of the sensitivity analysis are reported in Table 6. Table 6, *Panel A* shows that changes in the inflation rate of methane could potentially significantly affect the *NPV* in all scenarios. Results indicate that, regardless of the scenario or the fraction f, increasing the methane inflation rate from 2.5 % to 10 % leads to an improvement (a reduction in the absolute value of the negative *NPV*) of approximately 30 %. For this reason, it is provided in Figs. 4 and 5 the plots of the sensitivity analysis performed for the methane inflation rate for *daily* storage and *seasonal* storage. The figure shows the variation in *NPV* across different methane inflation rates relative to the benchmark *NPV* from the main analysis (with the inflation being 3 %). As the methane inflation rate rises, the *NPV* tends to increase, especially for larger values of *f*. Since, for each value of the methane inflation rate under analysis the full Monte Carlo simulation (i.e., the 10,000 replications) is repeated, the price of methane follows the distribution used in the main analysis.

Finally, the sensitivity of the discount rate is shown in Table 6, *Panel B*. Here, a less conservative range was chosen, i.e. the discount rate varied between 3 % and 8 %. It is also necessary to consider that, for green investments aimed at improving companies' sustainability practices, a lower discount rate should be recommended to give more weight to future cash flows and reduce the relative importance of initial outlays. The results obtained do not appear to be significantly affected by variations in the discount rate.

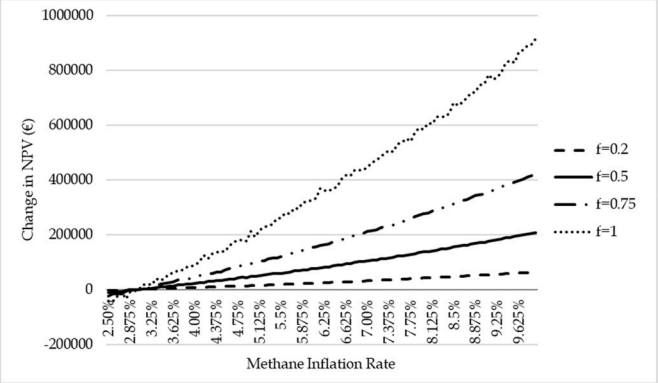

Fig. 4. Change in NPV for *daily* storage at different methane inflation rate.

4. Conclusions

This study evaluated the integration of green hydrogen produced via solar photovoltaic (PV) systems into the dairy industry, specifically as a substitute for methane in steam generation. The production of Parmigiano Reggiano cheese was selected as a representative example of a hard-to-abate industrial process, where hydrogen adoption could significantly contribute to decarbonization. Nevertheless, many of the findings from this analysis can be generalized to other thermal process applications. A range of scenarios was examined to assess the techno-economic feasibility of hydrogen implementation, accounting for variables such as PV system orientation (which may be limited by rooftop configuration), hydrogen storage pressure, and the hydrogen-to-methane volume ratio in fuel blends. Although the scenarios exhibit varying levels of profitability, none achieved a positive Net Present Value (*NPV*) over a 15-year analysis period. The most favorable

Table 6
Sensitivity analysis of the economic assessment on methane inflation rate (*Panel A*) and on the discount rate (*Panel B*).

Panel A: Sensitivity on methane inflation rate					
f	**Inflation rate interval**	**Benchmark**	**Min *NPV***	**Average**	**Max *NPV***
1	2.5 %; 10 %	−2,949,736.17 €	−2,991,008.25 €	−2,593,142.68 €	−2,090,705.50 €
***Daily* storage**					
f	**Inflation rate interval**	**Benchmark**	**Min *NPV***	**Average**	**Max *NPV***
0.2	2.5 %; 10 %	−217,797.53 €	−221,357.41 €	−192,508.45 €	−157,450.80 €
0.5	2.5 %; 10 %	−600,938.75 €	−612,573.13 €	−518,310.99 €	−403,765.34 €
0.75	2.5 %; 10 %	−1,108,072.07 €	−1,131,580.13 €	−941,138.82 €	−709,721.06 €
***Seasonal* storage**					
f	**Inflation rate interval**	**Benchmark**	**Min *NPV***	**Average**	**Max *NPV***
0.2	2.5 %; 10 %	−213,265.26 €	−216,391.53 €	−186,248.20 €	−148,182.14 €
0.5	2.5 %; 10 %	−750,748.50 €	−760,758.25 €	−664,262.55 €	−542,404.63 €
0.75	2.5 %; 10 %	−1,464,942.73 €	−1,485,161.50 €	−1,290,231.80 €	−1,044,065.19 €
Panel B: Sensitivity on the discount rate					
f	**Discount rate range**	**Benchmark**	**Min *NPV***	**Average**	**Max *NPV***
1	3 %; 8 %	−2,949,736.17 €	−3,363,894.25 €	−3,111,386.14 €	−2,787,470.50 €
***Daily* storage**					
f	**Discount rate range**	**Benchmark**	**Min *NPV***	**Average**	**Max *NPV***
0.2	3 %; 8 %	−217,797.53 €	−247,469.88 €	−229,376.08 €	−207,083.17 €
0.5	3 %; 8 %	−600,938.75 €	−694,059.88 €	−637,240.68 €	−567,618.25 €
0.75	3 %; 8 %	−1,108,072.07 €	−1,292,528.13 €	−1,179,944.53 €	−1,042,374.19 €
***Seasonal* storage**					
f	**Discount rate range**	**Benchmark**	**Min *NPV***	**Average**	**Max *NPV***
0.2	3 %; 8 %	−213,265.26 €	−244,282.67 €	−225,368.90 €	−201,128.75 €
0.5	3 %; 8 %	−750,748.50 €	−852,417.38 €	−790,442.22 €	−710,855.94 €
0.75	3 %; 8 %	−1,464,942.73 €	−1,668,526.75 €	−1,544,410.44 €	−1,385,146.25 €

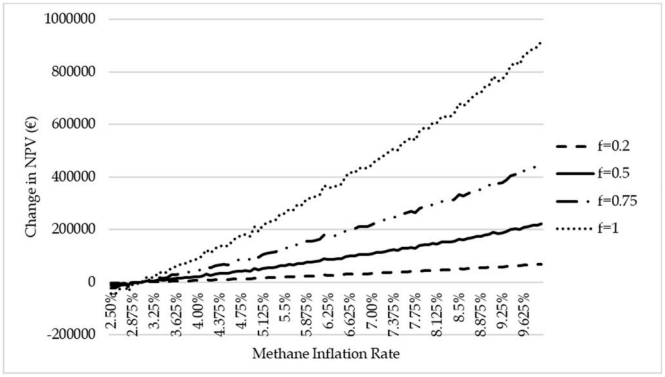

Fig. 5. Change in NPV for *seasonal* storage at different methane inflation rate.

outcomes occurred in scenarios that combined high inflation and methane prices, conditions under which hydrogen integration offers protection against market volatility. Still, the high capital expenditure (*CAPEX*) associated with hydrogen systems presents a major barrier. The most economically viable cases were those with lower investment requirements, particularly scenarios with a fuel blend ratio (f) of 0.2 and *seasonal* hydrogen storage, where a single boiler could be used for both hydrogen and methane, avoiding the need for duplicate infrastructure. Moreover, these scenarios offer the added value of allowing excess solar energy generated during high-irradiance months to be stored and utilized during periods of lower solar availability. This highlights the potential role of hydrogen as a seasonal energy carrier. Conversely, scenarios relying solely on hydrogen ($f = 1$) were the least profitable, despite offering the highest emissions savings (up to 400 tonnes of CO_{2eq}) annually, based on the production scale considered. However, the use of pure hydrogen also introduces operational risks, especially due to the potential for fuel supply interruptions, which could negatively impact both product quality and manufacturing continuity. In industries like dairy, where uninterrupted energy supply is critical, such risks must be carefully managed. Overall, the analysis highlights the vital role of public funding and policy incentives in supporting the economic viability of hydrogen-based transitions. For the investments evaluated, and over a 15-year time horizon, the emissions avoided per euro of public support range between 1.58 and 2.14 kg CO_{2eq}/€. The results underscore the economic challenges of using hydrogen for thermal process decarbonization under current cost and infrastructure conditions, particularly when compared to the low prevailing cost of fossil fuels such as methane. Limitations and future work: this study does not model potential regulatory constraints related to hydrogen storage and combustion; future work should incorporate permitting and compliance costs. In addition, comparative analyses with battery storage and high-temperature heat pumps, including partial and fully electric configurations, would further clarify the relative merits of alternative decarbonization pathways.

CRediT authorship contribution statement

Marco Puglia: Writing – review & editing, Writing – original draft, Visualization, Validation, Supervision, Methodology, Investigation, Formal analysis, Data curation, Conceptualization. **Simone Boccaletti:** Writing – review & editing, Writing – original draft, Visualization, Validation, Methodology, Investigation, Formal analysis, Data curation, Conceptualization. **Ahmet Fatih Kaya:** Writing – review & editing, Writing – original draft, Visualization, Validation, Software, Methodology, Investigation, Formal analysis, Data curation, Conceptualization. **Nicolò Morselli:** Writing – original draft, Validation, Methodology, Investigation, Data curation. **Giulio Allesina:** Writing – review & editing, Supervision, Investigation. **Simone Pedrazzi:** Writing – review & editing, Supervision, Investigation.

Declaration of generative AI and AI-assisted technologies in the writing process

During the preparation of this work the authors used OpenAI ChatGPT5 and Google Gemini in order to improve language, readability and to create some symbols in the graphical abstract. After using this tool/service, the authors reviewed and edited the content as needed and take full responsibility for the content of the publication.

Declaration of competing interest

The authors declare that they have no known competing financial interests or personal relationships that could have appeared to influence the work reported in this paper.

Acknowledgment

The authors would like to thank Jacopo Pavesi for his help with data collection.

Ahmet Fatih Kaya thanks the Ministry of National Education of Türkiye for funding the PhD at the University of Modena and Reggio Emilia.

This work was supperted by “Fondo di Ateneo per la Ricerca 2024 per il finanziamento di Piani di sviluppo dipartimentale nell’ambito della ricerca (E93C24000500005) (FARD 2024/2025), Department of Engineering Enzo Ferrari - University of Modena and Reggio Emilia.”

Appendix A Consideration on the surface extension of photovoltaic plant

Among the 36 *seasonal,* 36 *daily* and 12 fully hydrogen powered scenarios evaluated, considering an area of 1.748 m^2 per 350 W solar panel, the photovoltaic plant size ranges between a minimum of 748 m^2 and a maximum of 13,709 m^2. The largest surface corresponds to the scenario with a 12° tilt and 270° azimuth (west orientation). All scenarios modelled in this study are based on an annual production of 30,000 wheels of Parmigiano Reggiano, which requires approximately 16.5 million kg of milk, assuming that each wheel requires 550 kg of milk [42]. With an average daily milk yield of 35 kg per lactating cow, a herd of 1292 lactating cows is needed. Considering that in a typical Parmigiano Reggiano production system the herd structure is composed of 2.09 total heads per lactating cow (including dry cows, heifers, and calves), the total herd size is estimated at approximately 2700 heads. The space required to accommodate such a population varies depending on the housing system. Loose housing systems can provide up to 22 m^2 per cow [55], although a more common value for northern Italy is around 10.9 m^2 per cow [98]. Based on this more conservative estimation, the total roof area potentially available on barns would be approximately 29,430 m^2. Covering just the best-exposed half of this roof area with photovoltaic panels would be sufficient to meet the electricity demand assumed in this study, even under the worst-case orientation scenario.

Appendix B

Table B.1
Number of *PV* panels, electrolyser efficiency, new H_2 boiler *CAPEX*, and CH_4 and CO_{2eq} savings for different scenarios

Scenario number	N_{PV}	η_{el}, [%]	New H_2 Boiler CAPEX *Daily*	New H_2 Boiler CAPEX *Seasonal*	CH_4 savings [tonnes/year]	CO_{2eq} savings [tonnes/year]	CO_{2eq} savings [g_{CO2eq}/kg_{cheese}]*
1	451	74.21	66,499.20 €	0.00 €	9.5	29.7	28
2	428	74.22	66,499.20 €	0.00 €	9.5	29.7	28
3	467	74.21	67,382.40 €	0.00 €	9.5	29.7	28
4	443	74.21	67,382.40 €	0.00 €	9.5	29.7	28
5	492	74.4	69,840.00 €	0.00 €	9.5	29.7	28
6	467	74.4	69,840.00 €	0.00 €	9.5	29.7	28
7	499	74.37	70,070.40 €	0.00 €	9.5	29.7	28
8	474	74.36	70,070.40 €	0.00 €	9.5	29.7	28
9	522	74.37	71,068.80 €	0.00 €	9.5	29.7	28
10	495	74.38	71,068.80 €	0.00 €	9.5	29.7	28
11	576	75.37	73,334.40 €	0.00 €	9.5	29.7	28
12	546	75.38	73,334.40 €	0.00 €	9.5	29.6	28
13	1467	74.58	115,488.00 €	67,344.00 €	31.2	97.0	92
14	1401	74.08	115,424.40 €	67,344.00 €	31.2	97.0	92
15	1521	74.47	117,888.00 €	67,344.00 €	31.2	97.0	92
16	1451	74.07	117,792.00 €	67,344.00 €	31.2	97.0	92
17	1600	74.77	124,480.80 €	67,344.00 €	31.2	96.9	92
18	1521	74.66	124,544.40 €	67,344.00 €	31.2	97.0	92
19	1624	74.73	125,152.80 €	67,344.00 €	31.2	97.0	92
20	1551	74.22	125,120.40 €	67,344.00 €	31.2	97.0	92
21	1698	74.74	127,904.40 €	67,344.00 €	31.2	97.0	92
22	1613	74.63	127,904.40 €	67,344.00 €	31.2	96.9	92
23	1894	74.94	134,144.40 €	67,344.00 €	31.2	97.0	92
24	1800	74.83	134,144.40 €	67,344.00 €	31.2	97.0	92
25	2973	74.32	135,584.40 €	91,092.00 €	63.0	195.9	187
26	2833	74.01	135,584.40 €	91,092.00 €	63.0	195.9	187
27	3083	74.21	135,584.40 €	91,092.00 €	63.0	195.9	187
28	2934	74	135,584.40 €	91,092.00 €	63.0	195.9	187
29	3244	74.51	135,584.40 €	91,092.00 €	63.0	195.9	187
30	3091	74.2	135,584.40 €	91,092.00 €	63.0	195.9	187
31	3283	74.66	135,584.40 €	91,092.00 €	63.0	195.9	187
32	3120	74.56	135,584.40 €	91,092.00 €	63.0	195.9	187
33	3432	74.67	135,584.40 €	91,092.00 €	63.0	195.9	187
34	3270	74.37	135,584.40 €	91,092.00 €	63.0	195.9	187
35	3829	74.88	135,584.40 €	91,092.00 €	63.0	195.9	187
36	3648	74.59	135,584.40 €	91,092.00 €	63.0	195.9	187
37	6087	74.08	135,584.40 €	135,584.40 €	128.5	399.7	381
38	5776	74.08	135,584.40 €	135,584.40 €	128.5	399.7	381
39	6296	74.17	135,584.40 €	135,584.40 €	128.5	399.7	381
40	5974	74.18	135,584.40 €	135,584.40 €	128.5	399.7	381
41	6641	74.27	135,584.40 €	135,584.40 €	128.5	399.7	381
42	6303	74.27	135,584.40 €	135,584.40 €	128.5	399.7	381
43	6730	74.33	135,584.40 €	135,584.40 €	128.5	399.7	381
44	6387	74.33	135,584.40 €	135,584.40 €	128.5	399.7	381
45	7036	74.34	135,584.40 €	135,584.40 €	128.5	399.7	381
46	6667	74.34	135,584.40 €	135,584.40 €	128.5	399.7	381
47	7840	74.64	135,584.40 €	135,584.40 €	128.5	399.7	381
48	7440	74.64	135,584.40 €	135,584.40 €	128.5	399.7	381

* Assuming a wheel of Parmigiano Reggiano weighs 35 kg [99].

Appendix C

The amount of fugitive emissions associated with the analysed application falls within a range determined by the technology adopted in each stage of the natural gas supply chain. The *IPCC* provides emission factors corresponding to different technologies used in the various phases [100]. In particular, for natural gas exploration, emission factors range from 20.1 to 0.08 tonnes per million m^3 of gas, depending on whether operations occur without flaring or gas capture (onshore unconventional exploration) or with flaring or gas capture (onshore unconventional exploration). For production and gathering, emission factors range between 4.09 and 2.54 tonnes per million m^3 for onshore production, depending on whether higher- or lower-emitting technologies and practices are employed. For the gas processing segment, emission factors range from 1.83 to 0.75 tonnes per million m^3 of gas processed, depending on whether operations occur without LDAR, with limited LDAR and less than 50 % of centrifugal compressors using dry seals, or with extensive LDAR and at least 50 % of compressors using dry seals. For gas transmission, the range is 3.36 to 1.29 tonnes per million m^3 of gas, depending on whether the system employs limited or extensive LDAR and on the share of compressors equipped with dry seals. Regarding gas storage, emission factors range from 0.67 to 0.29 tonnes per million m^3 of gas consumed, depending on whether higher- or lower-emitting technologies and practices are predominant. By summing these contributions and considering a gas density of 0.718 kg/m^3, the resulting fugitive emissions range between 0.04185 and 0.00689 kg CH_4 emitted per kg CH_4 consumed. This range aligns with the estimate of 8700 tonnes CH_4 per billion m^3 (0.01212 kg CH_4 emitted per kg CH_4) for natural gas consumed in Europe, as reported by Shirizadeh et al. [101]. For subsequent calculations, this European value was adopted, as it represents the best fit, although year-to-year variations in the gas supply chain can lead to fluctuations in the carbon footprint of CH_4 utilization. Considering a GWP_{100} of 29.8, this corresponds to 0.36 kg of additional CO_2, leading to an overall GWP_{100} of

3.11 (2.75 kg from combustion and 0.36 kg from fugitive emissions). Other sources report significantly higher values, such as 5.6 and 6.2 [64,65]. Adopting a lower carbon footprint can therefore be regarded as a conservative assumption, particularly for economic assessments related to potential subsidies for avoided greenhouse gas emissions.

Appendix D

Table D.1
Economic assessment for $f = 0.2$ and different boiler efficiency (best scenario 2)

	Boiler Efficiency		
	90 %	92 %	Difference
Min *NPV*	−285,265.41 €	−278,082.34 €	−7183.07 €
Average *NPV*	−213,265.26 €	−211,505.95 €	−1759.31 €
Max *NPV*	−144,237.28 €	−142,386.94 €	−1850.34 €
Average Min *PFR*	71.74 %	72.18 %	−0.44 %
Average *ESPS*	1.72 $kgCO_{2eq}$/€	1.70 $kgCO_{2eq}$/€	0.02 $kgCO_{2eq}$/€

Data availability

The data and code required to reproduce the main results are openly available in Mendeley Data at https://doi.org/10.17632/rn9hw79dxj.1.

References

[1] Luqman M, Al-Ansari T. A novel solution towards zero waste in dairy farms: a thermodynamic study of an integrated polygeneration approach. Energy Convers Manag 2021;230:113753. https://doi.org/10.1016/j.enconman.2020.113753.

[2] Singaravadivelan A, Sachin PB, Harikumar S, Vijayakumar P, Vindhya MV, Farhana FMB, et al. Life cycle assessment of greenhouse gas emission from the dairy production system — review. Trop Anim Health Prod 2023;55:1–19. https://doi.org/10.1007/s11250-023-03748-4.

[3] Chinese D, Orrù PF, Meneghetti A, Cortella G, Giordano L, Benedetti M. Symbiotic and optimized energy supply for decarbonizing cheese production: an Italian case study. Energy 2022;257.

[4] Gosalvitr P, Cuellar-Franca R, Smith R, Azapagic A. Energy demand and carbon footprint of cheddar cheese with energy recovery from cheese whey. Energy Proc 2019;161:10–6. https://doi.org/10.1016/j.egypro.2019.02.052.

[5] Azadnia AH, McDaid C, Andwari AM, Hosseini SE. Green hydrogen supply chain risk analysis: a European hard-to-abate sectors perspective. Renew Sustain Energy Rev 2023;182:113371. https://doi.org/10.1016/j.rser.2023.113371.

[6] Mudhafar MAH, Zayed ME, Rehman S. Offshore wind-to-green hydrogen: a comprehensive review on current challenges, techno-economic analyses, environmental implications, and potential risks. Process Saf Environ Prot 2025; 201:107631. https://doi.org/10.1016/j.psep.2025.107631.

[7] Mostafaeipour A, Rezaei M, Moftakharzadeh A, Qolipour M, Salimi M. Evaluation of hydrogen production by wind energy for agricultural and industrial sectors. Int J Hydrogen Energy 2019;44:7983–95. https://doi.org/10.1016/j.ijhydene.2019.02.047.

[8] Rehman S, Kotb KM, Zayed ME, Menesy AS, Irshad K, Alzahrani AS, et al. Techno-economic evaluation and improved sizing optimization of green hydrogen production and storage under higher wind penetration in Aqaba gulf. J Energy Storage 2024;99:113368. https://doi.org/10.1016/j.est.2024.113368.

[9] Minh PV, Phuong LN, Hoai NN, Hong AN, Thi HP, Thanh TN, et al. Optimization study of green hydrogen fuel production stations in renewable energy hub: a case study in Quang Tri province, Vietnam. Int J Hydrogen Energy 2025;151:150204. https://doi.org/10.1016/j.ijhydene.2025.150204.

[10] Shboul B, Zayed ME, Tariq R, Ashraf WM, Odat AS, Rehman S, et al. New hybrid photovoltaic-fuel cell system for green hydrogen and power production: performance optimization assisted with gaussian process regression method. Int J Hydrogen Energy 2024;59:1214–29. https://doi.org/10.1016/j.ijhydene.2024.02.087.

[11] Abd Elaziz M, Senthilraja S, Zayed ME, Elsheikh AH, Mostafa RR, Lu S. A new random vector functional link integrated with mayfly optimization algorithm for performance prediction of solar photovoltaic thermal collector combined with electrolytic hydrogen production system. Appl Therm Eng 2021;193:117055. https://doi.org/10.1016/j.applthermaleng.2021.117055.

[12] Vance C, Maimó Far A, Sweeney C, Syron E. Techno-economic optimization of green hydrogen production from curtailed power in Ireland: impact of future renewable energy installations, weather variability, and grid constraints. Int J Hydrogen Energy 2025;161. https://doi.org/10.1016/j.ijhydene.2025.150675.

[13] Okonkwo PC, Islam MS, Taura UH, Barhoumi EM, Mansir IB, Das BK, et al. A techno-economic analysis of renewable hybrid energy systems for hydrogen production at refueling stations. Int J Hydrogen Energy 2024;78:68–82. https://doi.org/10.1016/j.ijhydene.2024.06.294.

[14] Yamaguchi S, Takahashi Y, Hayashi T. Small indoor hydroponic system with renewable energy. In: Int conf control autom syst 2018; 2018-Octob. p. 313–8.

[15] Nguyen NT, Matsuhashi R. An optimal design on sustainable energy systems for shrimp farms. IEEE POWER ENERGY Soc Sect 2019;7:165543–58. https://doi.org/10.1109/ACCESS.2019.2952923.

[16] Carroquino J, Bernal-Agustín JL, Dufo-López R. Standalone renewable energy and hydrogen in an agricultural context: a demonstrative case. Sustain Times 2019; 11. https://doi.org/10.3390/su11040951.

[17] Farhani S, Barhoumi EM, Ul Islam Q, Becha F. Optimal design and economic analysis of a stand-alone integrated solar hydrogen water desalination system case study agriculture farm in Kairouan Tunisia. Int J Hydrogen Energy 2024;63: 759–66. https://doi.org/10.1016/j.ijhydene.2024.03.043.

[18] Temiz M, Dincer I. Development of concentrated solar and agrivoltaic based system to generate water, food and energy with hydrogen for sustainable agriculture. Appl Energy 2024;358:122539. https://doi.org/10.1016/j.apenergy.2023.122539.

[19] Janke L, McDonagh S, Weinrich S, Nilsson D, Hansson PA, Nordberg Å. Techno-economic assessment of demand-driven small-scale green hydrogen production for low carbon agriculture in Sweden. Front Energy Res 2020;8:1–19. https://doi.org/10.3389/fenrg.2020.595224.

[20] Ceylan C, Devrim Y. Design and simulation of the PV/PEM fuel cell based hybrid energy system using MATLAB/simulink for greenhouse application. Int J Hydrogen Energy 2021;46:22092–106. https://doi.org/10.1016/j.ijhydene.2021.04.034.

[21] Al-Ali H, Ali D, Atteya AI. Investigating the potential of renewable-hydrogen energy storage systems (RHES) in enabling scotland's farming communities net-zero transition and sizing the proposed RHES system. Green Energy Environ Technol 2023:1–32.

[22] Hadjiat MM, Mraoui A, Ouali S, Kuzgunkaya EH, Salhi K, Ait Ouali A, et al. Assessment of geothermal energy use with thermoelectric generator for hydrogen production. Int J Hydrogen Energy 2021;46:37545–55. https://doi.org/10.1016/j.ijhydene.2021.06.130.

[23] Karayel GK, Javani N, Dincer I. Effective use of geothermal energy for hydrogen production: a comprehensive application. Energy 2022;249:123597. https://doi.org/10.1016/j.energy.2022.123597.

[24] Yang X, Zhang H, Zhang Z, Li Y, Liu H, Zhang F, et al. Enhanced bio-hydrogen production by photo-fermentation of corn stalk using Fe-doped CaTiO3 photocatalyst. Energy 2024;301:131682. https://doi.org/10.1016/j.energy.2024.131682.

[25] Cook B, Hagen C. Techno-economic analysis of biomass gasification for hydrogen production in three US-based case studies. Int J Hydrogen Energy 2024;49: 202–18. https://doi.org/10.1016/j.ijhydene.2023.07.219.

[26] Gubin V, Benedikt F, Thelen F, Hammerschmid M, Popov T, Hofbauer H, et al. Hydrogen production from woody biomass gasification: a techno-economic analysis. Biofuel Bioprod Biorefining 2024;18:818–36. https://doi.org/10.1002/bbb.2647.

[27] Schiro F, Stoppato A, Benato A. Modelling and analyzing the impact of hydrogen enriched natural gas on domestic gas boilers in a decarbonization perspective. Carbon Resour Convers 2020;3:122–9. https://doi.org/10.1016/j.crcon.2020.08.001.

[28] Wang T, Zhang H, Zhang Y, Wang H, Lyu J, Yue G. Efficiency and emissions of gas-fired industrial boiler fueled with hydrogen-enriched nature gas: a case study of 108 t/h steam boiler. Int J Hydrogen Energy 2022;47:28188–203. https://doi.org/10.1016/j.ijhydene.2022.06.121.

[29] Bălănescu DT, Homutescu VM. Effects of hydrogen-enriched methane combustion on latent heat recovery potential and environmental impact of condensing boilers. Appl Therm Eng 2021;197. https://doi.org/10.1016/j.applthermaleng.2021.117411.

[30] Yang H, Lin X, Pan H, Geng S, Chen Z, Liu Y. Energy saving analysis and thermal performance evaluation of a hydrogen-enriched natural gas-fired condensing boiler. Int J Hydrogen Energy 2023;48:19279–96. https://doi.org/10.1016/j.ijhydene.2023.02.027.
[31] Cellek MS, Pınarbaşı A. Investigations on performance and emission characteristics of an industrial low swirl burner while burning natural gas, methane, hydrogen-enriched natural gas and hydrogen as fuels. Int J Hydrogen Energy 2018;43:1194–207. https://doi.org/10.1016/j.ijhydene.2017.05.107.
[32] Xin Y, Wang K, Zhang Y, Zeng F, He X, Takyi SA, et al. Numerical simulation of combustion of natural gas mixed with hydrogen in gas boilers. Energies 2021;14. https://doi.org/10.3390/en14216883.
[33] Boulahlib MS, Medaerts F, Boukhalfa MA. Experimental study of a domestic boiler using hydrogen methane blend and fuel-rich staged combustion. Int J Hydrogen Energy 2021;46:37628–40. https://doi.org/10.1016/j.ijhydene.2021.01.103.
[34] Wang T, Liu X, Zhang Y, Zhang H. Thermodynamic and emission characteristics of a hydrogen-enriched natural gas-fired boiler integrated with external flue gas recirculation and waste heat recovery. Appl Energy 2024;358:122614. https://doi.org/10.1016/j.apenergy.2023.122614.
[35] Cheng L, Li W, Peng S, Chai C, Wang W, Tian C, et al. Study of combustion characteristics of hydrogen-doped natural gas in industrial boilers. Int J Hydrogen Energy 2024;92:590–604. https://doi.org/10.1016/j.ijhydene.2024.10.279.
[36] Hillmann H, Hofmann T. Quantitation of key tastants and Re-engineering the taste of parmesan cheese. J Agric Food Chem 2016;64:1794–805. https://doi.org/10.1021/acs.jafc.6b00112.
[37] Consorzio. Consortium of Parmigiano Reggiano. Specification as in force from march 30, 2018, production specifications for parmigiano reggiano cheese, parmigiano reggiano cheese production standards n.d. https://backend.parmigianoreggiano.com/uploads/0325_disciplinare_docx_EN_2eda3456af.pdf. [Accessed 29 November 2024].
[38] Karthikeyan B, Praveen Kumar G. Thermoeconomic and optimization approaches for integrating cooling, power, and green hydrogen production in dairy plants with a novel solar-biomass cascade ORC system. Energy Convers Manag 2023;295:117645. https://doi.org/10.1016/j.enconman.2023.117645.
[39] Maganza A, Gabetti A, Pastorino P, Zanoli A, Sicuro B, Barcelò D, et al. Toward sustainability: an overview of the use of green hydrogen in the agriculture and livestock sector. Animals 2023;13:1–15. https://doi.org/10.3390/ani13162561.
[40] Miserocchi L, Franco A, Testi D. A novel approach to energy management in the dairy industry using performance indicators and load profiles: application to a cheese dairy plant in tuscany, Italy. Energy 2024;310:133240. https://doi.org/10.1016/j.energy.2024.133240.
[41] PR. Regolamento applicativo QLPR triennio 2023-2025. Decreto 11 luglio 2022 n. 308337 n.d. https://registro.parmigianoreggiano.it/qlpr/linkDocument?n=REGOLAMENTO+APPLICATIVO+2023-2025+-+30.03.23.pdf&a=true&f=true&d=true. [Accessed 2 December 2024].
[42] Pietri A, Mulazzi A, Piva G, Bertuzzi T. Fate of aflatoxin M1 during production and storage of parmesan cheese. Food Control 2016;60:478–83. https://doi.org/10.1016/j.foodcont.2015.08.032.
[43] Popping B, De Dominicis E, Dante M, Nocetti M. Identification of the geographic origin of parmigiano reggiano (P.d.o.) cheeses deploying non-targeted mass spectrometry and chemometrics. Foods 2017;6:1–7. https://doi.org/10.3390/foods6020013.
[44] UNI. UNI/TS 11854:2022 2022. https://store.uni.com/uni-ts-11854-2022. [Accessed 7 April 2025].
[45] Williams L, Mckenzie-Brook T, Lee R, Lewis E, Proud W, Taylor S, et al. Technical feasibility of hydrogen boilers in homes. 2023. Report For Environmental Coalition on Standards (ECOS). Bristol, United Kingdom.
[46] Photovoltaic geographical information system (PVgis) n.d. https://re.jrc.ec.europa.eu/pvg_tools/en/.
[47] Elazab R, Daowd M. New geographic information system based sustainability metric for isolated photovoltaic systems. Sci Rep 2025;15:2023. https://doi.org/10.1038/s41598-025-85222-9.
[48] Kulesza K, Martinez A, Taylor N. Assessment of typical meteorological year data in photovoltaic geographical information system 5.2, based on reanalysis and ground station data from 147 European weather stations. Atmosphere 2023;14. https://doi.org/10.3390/atmos14121803.
[49] Gbémou S, Eynard J, Thil S, Guillot E, Grieu S. A comparative study of machine learning-based methods for global horizontal irradiance forecasting. Energies 2021;14:1–23. https://doi.org/10.3390/en14113192.
[50] Mukeshimana MC, Zhao ZY, Nshimiyimana JP. Techno-economic analysis and viability assessment of concentrating solar power under climatic conditions of Rwanda. Int J Energy Water Resour 2022;6:277–93. https://doi.org/10.1007/s42108-021-00161-1.
[51] Blair N, Diorio N, Freeman J, Gilman P, Janzou S, Neises TW, et al. System advisor model (SAM) general description. 2018.
[52] Esparza I, Olábarri Candela Á, Huang L, Yang Y, Budiono C, Riyadi S, et al. Floating PV systems as an alternative power source: case study on three representative islands of Indonesia. Sustain Times 2024;16. https://doi.org/10.3390/su16031345.
[53] Akello POO, Saoke CO, Kamau JN, Ndeda JOH. Modeling and performance analysis of solar parabolic trough collectors for hybrid process heat application in Kenya's tea industry using system advisor model. Sustain Energy Res 2023;10. https://doi.org/10.1186/s40807-023-00077-w.
[54] Khan SUD, Wazeer I, Almutairi Z. Comparative analysis of SAM and RETScreen tools for the case study of 600 kW solar PV system installation in Riyadh, Saudi Arabia. Sustain Times 2023;15. https://doi.org/10.3390/su15065381.
[55] Shoshani E, Hetzroni A. Optimal barn characteristics for high-yielding holstein cows as derived by a new heat-stress model. Animal 2013;7:176–82. https://doi.org/10.1017/S1751731112001085.
[56] Magarelli A, Mazzeo A, Ferrara G. Fruit crop species with agrivoltaic systems: a critical review. Agronomy 2024;14. https://doi.org/10.3390/agronomy14040722.
[57] Amaducci S, Yin X, Colauzzi M. Agrivoltaic systems to optimise land use for electric energy production. Appl Energy 2018;220:545–61. https://doi.org/10.1016/j.apenergy.2018.03.081.
[58] Gambou F, Guilbert D, Zasadzinski M, Rafaralahy H. A comprehensive survey of alkaline electrolyzer modeling: electrical domain and specific electrolyte conductivity. Energies 2022;15. https://doi.org/10.3390/en15093452.
[59] Ulleberg Ø. Modeling of advanced alkaline electrolyzers a system. Hydrog Energy 2003;28:21–33.
[60] Pedrazzi S, Zini G, Tartarini P. Modelling and simulation of a wind-hydrogen CHP system with metal hydride storage. Renew Energy 2012;46:14–22. https://doi.org/10.1016/j.renene.2012.03.004.
[61] Kaya AF, Morselli N, Puglia M, Allesina G, Pedrazzi S. Design optimization of two-blade savonius wind turbines for hydrogen generation. Renew Energy 2024;231. https://doi.org/10.1016/j.renene.2024.121028.
[62] Tijani AS, Yusup NAB, Rahim AHA. Mathematical modelling and simulation analysis of advanced alkaline electrolyzer system for hydrogen production. Procedia Technol 2014;15:798–806. https://doi.org/10.1016/j.protcy.2014.09.053.
[63] Barthels H, Brocke WA, Bonhoff K, Groehn HG, Heuts G, Lennartz M, et al. PHOEBUS-Jülich: an autonomous energy supply system comprising photovoltaics, electrolytic hydrogen, fuel cell. Int J Hydrogen Energy 1998;23:295–301. https://doi.org/10.1016/s0360-3199(97)00055-4.
[64] Mergel J. Personal communication. PHOEBUS electrolyzer: detailed operational data. FZJ—Forschungszentrum; 1997.
[65] Jadhav S, Devdas N, Nisar S, Bajpai V. Bidirectional DC-DC converter in solar PV system for battery charging application. In: 2018 int conf smart city emerg technol ICSCET; 2018. p. 1–4. https://doi.org/10.1109/ICSCET.2018.8537391. 2018.
[66] Kim H sung, Kim JH, Min BD, Yoo DW, Kim HJ. A highly efficient PV system using a series connection of DC-DC converter output with a photovoltaic panel. Renew Energy 2009;34:2432–6. https://doi.org/10.1016/j.renene.2009.01.011.
[67] Elmasry Y, Mansir IB, Abubakar Z, Ali A, Aliyu S, Almamun K. Electricity-hydrogen nexus integrated with multi-level hydrogen storage, solar PV site, and electric-fuelcell car charging stations. Int J Hydrogen Energy 2024;76:160–71. https://doi.org/10.1016/j.ijhydene.2024.02.222.
[68] Temiz M, Dincer I. Techno-economic analysis of green hydrogen ferries with a floating photovoltaic based marine fueling station. Energy Convers Manag 2021;247:114760. https://doi.org/10.1016/j.enconman.2021.114760.
[69] Meratizaman M, Monadizadeh S, Amidpour M. Simulation, economic and environmental evaluations of green solar parking (refueling station) for fuel cell vehicle. Int J Hydrogen Energy 2014;39:2359–73. https://doi.org/10.1016/j.ijhydene.2013.11.094.
[70] Martire M, Kaya AF, Morselli N, Puglia M, Allesina G, Pedrazzi S. Analysis and optimization of a hybrid system for the production and use of green hydrogen as fuel for a commercial boiler. Int J Hydrogen Energy 2024;56:769–79. https://doi.org/10.1016/j.ijhydene.2023.12.223.
[71] Arslan O. Performance analysis of a novel heat recovery system with hydrogen production designed for the improvement of boiler effectiveness. Int J Hydrogen Energy 2021;46:7558–72. https://doi.org/10.1016/j.ijhydene.2020.11.253.
[72] Khan MA, Young C, Mackinnon CB, Layzell DB. The techno-economics of hydrogen compression. Transit Accel Tech Briefs 2021;1:1–36.
[73] Roslyakov PV, Proskurin YV, Ionkin IL. Increase of efficiency and reliability of liquid fuel combustion in small-sized boilers. J Phys Conf Ser 2017;891. https://doi.org/10.1088/1742-6596/891/1/012243.
[74] Kalinci Y, Hepbasli A, Dincer I. Efficiency assessment of an integrated gasifier/boiler system for hydrogen production with different biomass types. Int J Hydrogen Energy 2010;35:4991–5000. https://doi.org/10.1016/j.ijhydene.2009.08.079.
[75] Armour K, et al. The earth's energy budget, climate feedbacks and climate sensitivity. AGU Fall Meeting Abstracts; 2021. https://doi.org/10.1017/9781009157896.009.
[76] Jung W, Cho S, Choi Y, Lee H, Na JG, Lee J. Methane capture, utilization, and sequestration technology based on biological ectoine production using Methylotuvimicrobium alcaliphilum 20Z. Chem Eng J 2024;498:155339. https://doi.org/10.1016/j.cej.2024.155339.
[77] Benalcazar P, Komorowska A. Prospects of green hydrogen in Poland: a techno-economic analysis using a monte carlo approach. Int J Hydrogen Energy 2022;47:5779–96. https://doi.org/10.1016/j.ijhydene.2021.12.001.
[78] Hassani H, Zaouche F, Rekioua D, Belaid S, Rekioua T, Bacha S. Feasibility of a standalone photovoltaic/battery system with hydrogen production. J Energy Storage 2020;31:101644. https://doi.org/10.1016/j.est.2020.101644.
[79] Reddi K, Elgowainy A, Rustagi N, Gupta E. Impact of hydrogen refueling configurations and market parameters on the refueling cost of hydrogen. Int J Hydrogen Energy 2017;42:21855–65. https://doi.org/10.1016/j.ijhydene.2017.05.122.
[80] Apostolou D, Enevoldsen P, Xydis G. Supporting green urban mobility – the case of a small-scale autonomous hydrogen refuelling station. Int J Hydrogen Energy 2019;44:9675–89. https://doi.org/10.1016/j.ijhydene.2018.11.197.
[81] Zghaibeh M, Barhoumi EM, Okonkwo PC, Ben Belgacem I, Beitelmal WH, Mansir IB. Analytical model for a techno-economic assessment of green hydrogen

production in photovoltaic power station case study salalah city-Oman. Int J Hydrogen Energy 2022;47:14171–9. https://doi.org/10.1016/j.ijhydene.2022.02.180.
[82] Schmidt O, Gambhir A, Staffell I, Hawkes A, Nelson J, Few S. Future cost and performance of water electrolysis: an expert elicitation study. Int J Hydrogen Energy 2017;42:30470–92. https://doi.org/10.1016/j.ijhydene.2017.10.045.
[83] Wei X, Sharma S, Waeber A, Wen D, Sampathkumar SN, Margni M, et al. Comparative life cycle analysis of electrolyzer technologies for hydrogen production: manufacturing and operations. Joule 2024;8:3347–72. https://doi.org/10.1016/j.joule.2024.09.007.
[84] Allouhi A, Buker MS, El-houari H, Boharb A, Benzakour Amine M, Kousksou T, et al. PV water pumping systems for domestic uses in remote areas: sizing process, simulation and economic evaluation. Renew Energy 2019;132:798–812. https://doi.org/10.1016/j.renene.2018.08.019.
[85] Mongird K, Viswanathan V, Alam J, Vartanian C, Sprenkle V, Baxter R. 2020 grid energy storage technology cost and performance assessment. 2020.
[86] Zhang X, Wei QS, Oh BS. Cost analysis of off-grid renewable hybrid power generation system on Ui island, South Korea. Int J Hydrogen Energy 2022;47:13199–212. https://doi.org/10.1016/j.ijhydene.2022.01.150.
[87] Liu H, Zhai R, Fu J, Wang Y, Yang Y. Optimization study of thermal-storage PV-CSP integrated system based on GA-PSO algorithm. Sol Energy 2019;184:391–409. https://doi.org/10.1016/j.solener.2019.04.017.
[88] IRENA International Renewable Energy Agency. Low-cost finance for the energy transition. 2023.
[89] Urs RR, Chadly A, Al Sumaiti A, Mayyas A. Techno-economic analysis of green hydrogen as an energy-storage medium for commercial buildings. Clean Energy 2023;7:84–98. https://doi.org/10.1093/ce/zkac083.
[90] Barhoumi EM, Okonkwo PC, Ben Belgacem I, Zghaibeh M, Tlili I. Optimal sizing of photovoltaic systems based green hydrogen refueling stations case study Oman. Int J Hydrogen Energy 2022;47:31964–73. https://doi.org/10.1016/j.ijhydene.2022.07.140.
[91] Shakya BD, Aye L, Musgrave P. Technical feasibility and financial analysis of hybrid wind-photovoltaic system with hydrogen storage for cooma. Int J Hydrogen Energy 2005;30:9–20. https://doi.org/10.1016/j.ijhydene.2004.03.013.
[92] Lee B, Chae H, Choi NH, Moon C, Moon S, Lim H. Economic evaluation with sensitivity and profitability analysis for hydrogen production from water electrolysis in Korea. Int J Hydrogen Energy 2017;42:6462–71. https://doi.org/10.1016/j.ijhydene.2016.12.153.
[93] Le Duigou A, Bader AG, Lanoix JC, Nadau L. Relevance and costs of large scale underground hydrogen storage in France. Int J Hydrogen Energy 2017;42:22987–3003. https://doi.org/10.1016/j.ijhydene.2017.06.239.
[94] Liu B, Liu S, Guo S, Zhang S. Economic study of a large-scale renewable hydrogen application utilizing surplus renewable energy and natural gas pipeline transportation in China. Int J Hydrogen Energy 2020;45:1385–98. https://doi.org/10.1016/j.ijhydene.2019.11.056.
[95] EUROSTAT n.d. https://ec.europa.eu/eurostat/statistics-explained/index.php?title=Natural_gas_price_statistics.
[96] El-Hadary MI, Senthilraja S, Zayed ME. A hybrid system coupling spiral type solar photovoltaic thermal collector and electrocatalytic hydrogen production cell: experimental investigation and numerical modeling. Process Saf Environ Prot 2023;170:1101–20. https://doi.org/10.1016/j.psep.2022.12.079.
[97] Liu J, Serletis A. Volatility and dependence in energy markets. J Econ Finance 2023;47:15–37. https://doi.org/10.1007/s12197-022-09609-4.
[98] Leso L, Uberti M, Morshed W, Barbari M. A survey on Italian compost dairy barns. J Agric Eng 2013;44. https://doi.org/10.4081/jae.2013.s2.e40.
[99] Franceschi P, Malacarne M, Formaggioni P, Cipolat-Gotet C, Stocco G, Summer A. Effect of season and factory on cheese-making efficiency in parmigiano reggiano manufacture. Foods 2019;8. https://doi.org/10.3390/foods8080315.
[100] Intergovernmental Panel on Climate Change. Chapter 4: fugitive emissions. In: 2019 refinement to the 2006 IPCC guidelines for national greenhouse gas inventories, vol. 2; 2024. Energy. n.d.
[101] Shirizadeh B, Villavicencio M, Douguet S, Trüby J, Bou Issa C, Seck GS, et al. The impact of methane leakage on the role of natural gas in the European energy transition. Nat Commun 2023;14:1–4. https://doi.org/10.1038/s41467-023-41527-9.